Title

NUCLEAR LOCALIZATION AND PHOSPHORYLATION MODULATE PATHOLOGICAL EFFECTS OF ALPHA-SYNUCLEIN

Authors

Raquel Pinho[1,2], Isabel Paiva[1], Kristina Gotovac Jerčić[3], Luis Fonseca-Ornelas[4], Ellen Gerhardt[1], Christiane Fahlbusch[1], Paula Garcia-Esparcia[5], Cemil Kerimoglu[6], Maria A. Pavlou[1], Anna Villar-Piqué[1], Éva Szegő[1], Tomás Lopes da Fonseca[1], Francesca Odoardi[7], Szabolcs Soeroes[8,9], Ana Cristina Rego[10], Wolfgang Fischle[8,11], Jens C. Schwamborn[12], Thomas Meyer[13], Sebastian Kügler[14], Isidre Ferrer[5], Johannes Attems[15], André Fischer[6,16], Stefan Becker[4], Markus Zweckstetter[4,14,17], Fran Borovecki[3,18], and Tiago F Outeiro[1,15, 19,20] *

Affiliations

[1]Department of Experimental Neurodegeneration, Center for Biostructural Imaging of Neurodegeneration, Center for Nanoscale Microscopy and Molecular Physiology of the Brain, University Medical Center Göttingen, 37073, Göttingen, Germany

[2]Faculty of Medicine, University of Porto, 4200 – 319, Porto, Portugal

[3]Department for Functional Genomics, Center for Translational and Clinical Research, University Hospital Center Zagreb, University of Zagreb School of Medicine, 10 000, Zagreb, Croatia

[4]Max Planck Institute for Biophysical Chemistry, 37077, Göttingen, Germany

[5]Institute of Neuropathology, Bellvitge University Hospital, University of Barcelona, Bellvitge Biomedical Research Institute, Hospitalet de Llobregat; Biomedical Research Center of Neurodegenerative Diseases, 08908, Barcelona, Spain

[6]Department for Psychiatry and Psychotherapy, University Medical Center, 37075, Göttingen, Germany

[7]Institute of Neuroimmunology and Institute for Multiple Sclerosis Research, University Medical Centre Göttingen, 37073, Göttingen, Germany

[8]Max Planck Institute for Biophysical Chemistry, Laboratory of Chromatin Biochemistry, 37077, Göttingen, Germany

[9]Oxford Nanopore Technologies LTD, OX4 4DQ, Oxford, United Kingdom

[10]Center for Neuroscience and Cell Biology and Faculty of Medicine, University of Coimbra, 3004-517, Coimbra, Portugal

[11]King Abdullah University of Science and Technology (KAUST), Environmental Epigenetics Program, 23955, Thuwal, Saudi Arabia

[12]Development and Cellular Biology, Luxembourg Centre for Systems Biomedicine (LCSB), University of Luxembourg, 2721, Esch-sur-Alzette, Luxembourg

[13]Klinik für Psychosomatische Medizin und Psychotherapie, Universitätsmedizin Göttingen, 37073, Göttingen, Germany

[14]Department of Neurology, Center for Nanoscale Microscopy and Molecular Physiology of the Brain, University Medical Center Göttingen, 37073, Göttingen, Germany

[15]Institute of Neuroscience, Newcastle University, Campus for Ageing and Vitality, NE1 7RU, Newcastle upon Tyne, United Kingdom

[16]Department of Epigenetics and Systems Medicine in Neurodegenerative Diseases, German Center for Neurodegenerative Diseases (DZNE), Göttingen, Germany

[17]Structural Biology in Dementia, German Center for Neurodegenerative Diseases (DZNE), 37075, Göttingen, Germany

[18]Department of Neurology, University Hospital Center Zagreb, 10 000, Zagreb, Croatia

[19]Chronic Disease Research Center (CEDOC), NOVA Medical School, 1150-082, Lisboa, Portugal

[20]Max Planck Institute for Experimental Medicine, 37075, Göttingen, Germany

Corresponding author

Prof. Dr. Tiago Fleming Outeiro

Department of Experimental Neurodegeneration

University Medical Center Göttingen

Waldweg 33

37073 Göttingen

Germany

Phone: +495513913544

Fax: +495513922693

E-mail: touteir@gwdg.de

Abstract

Alpha-synuclein (aSyn) is a central player in Parkinson's disease (PD) but the precise molecular mechanisms underlying its pathogenicity remain unclear. It has recently been suggested that nuclear aSyn may modulate gene expression, possibly via interactions with DNA. However, the biological behavior of aSyn in the nucleus and

3

the factors affecting its transcriptional role are not known. Here, we investigated the mechanisms underlying aSyn-mediated transcription deregulation by assessing its effects in the nucleus and the impact of phosphorylation in these dynamics. We found that aSyn induced severe transcriptional deregulation, including the downregulation of important cell cycle-related genes. Importantly, transcriptional deregulation was concomitant with reduced binding of aSyn to DNA. By forcing the nuclear presence of aSyn in the nucleus (aSyn-NLS), we found the accumulation of high molecular weight aSyn species altered gene expression and reduced toxicity when compared to the wild-type or exclusively cytosolic protein. Interestingly, nuclear localization of aSyn, and the effect on gene expression and cytotoxicity, was also modulated by phosphorylation on serine 129. Thus, we hypothesize that the role of aSyn on gene expression and, ultimately, toxicity, may be modulated by the phosphorylation status and nuclear presence of different aSyn species. Our findings shed new light onto the subcellular dynamics of aSyn and unveil an intricate interplay between subcellular location, phosphorylation, and toxicity, opening novel avenues for the design of future strategies for therapeutic intervention in PD and other synucleinopathies.

Introduction

Alpha-synuclein (aSyn) is associated with both familial and sporadic forms of Parkinson's Disease (PD) (1, 2), and is a main component of proteinaceous inclusions, known as Lewy bodies or neurites, found in the brains of patients with PD or other Lewy body disease (3). In recent years, important progress has been made towards our understanding of aSyn biology, but major questions regarding its function remain unanswered.

4

Recent reports suggested a possible role of aSyn in transcriptional regulation (4, 5), a vital cellular mechanism found deregulated in PD patients (6, 7) and in mouse models of the disease (8). The occurrence of aSyn in the nucleus is controversial (9, 10), but accumulating evidence supports the presence of different aSyn species in the nucleus of neuronal cells in the brain of PD patients (11-13), and in mouse and cellular models of the disease (11, 14-16). However, the effects of aSyn in the nucleus are vastly unknown. Few studies suggest that stress increases the nuclear levels of aSyn (14, 17-19), but the factors underlying its translocation into the nucleus are unclear. Phosphorylation of aSyn at serine S129 (pS129) is also suspected to interfere with its subcellular localization, but it is not clear whether it enhances (20-23) or decreases (24) nuclear localization.

The mechanisms behind aSyn-induced transcriptional deregulation are also not clear, but sporadic reports suggest that nuclear aSyn binds histones, and/or modulates histone acetylation levels (14, 17, 18), and specific DNA regions (11, 25). A stimulatory effect of nucleic acids (26) and nuclear factors (17, 27) on aSyn fibrillation was previously reported, which imply that interaction of aSyn with DNA or other nuclear partners may alter the protein conformation and, eventually, its toxicity. There is no consensus on whether the presence of aSyn in the nucleus is protective or cytotoxic. While some studies reported that nuclear aSyn promotes toxicity, by inhibiting histone acetylation (14) or affecting cell cycle regulation (19), others observed increased cellular protection against stress , via histone hyperacetylation and modulation of DNA replication (18). Posttranslational modifications (PTMs) of aSyn are also known to affect its toxicity. S129 phosphorylation has been linked to both protective and toxic roles (28-31), but its effect on nuclear aSyn is unknown.

5

We have recently reported on a strong effect of aSyn on transcription (32, 33), and highlighted different cellular mechanisms modulated by wild-type (WT) and mutant A30P aSyn - such as DNA damage and ER-Golgi systems, respectively. We have also shown that mutant A30P aSyn binds to more DNA regions compared to the endogenous aSyn, corroborating the hypothesis that aSyn-DNA binding might be a relevant mechanism underlying neurotoxicity (33). Thus, further understanding the interaction between aSyn and DNA, and the factors modulating its import and function in the nucleus is critical. Here, we also studied the effect of aSyn on gene expression. Our findings indicate that nuclear WT aSyn promotes severe alterations in gene expression, including downregulation of cell cycle-related genes. Importantly, transcriptional deregulation was associated with lower binding of aSyn to DNA, in both cellular and transgenic mouse models of PD. In human cells, targeting aSyn to the nucleus using a nuclear localization sequence (aSyn-NLS) induced conformational changes that were concomitant with gene expression alterations in cell-cycle genes, and reduced cell damage. Excitingly, we found that pS129 is not only important for the subcellular localization of the protein, but may also regulate aSyn function and toxicity in a subcellular localization-dependent manner. While blocking aSyn S129 phosphorylation resulted in an up-regulation of genes regulated by aSyn and decreased toxicity, blocking aSyn-NLS S129 phosphorylation promoted downregulation of those genes and caused cell damage.

To the best of our knowledge, this is the first study directly addressing the role of pS129 on the nuclear localization of aSyn. Alterations in the nuclear content of aSyn, thereby modulating its effects on transcription, may be involved in aSyn pathobiology. Ultimately, studies aimed at furthering our understanding of the role of

6

aSyn in the nucleus will pave the way for identification of novel targets for therapeutic intervention in PD and other synucleinopathies.

Results

aSyn induces transcriptional deregulation of cell cycle-related genes

Lund human mesencephalic (LUHMES) cells can be differentiated into neuronal cells with a robust dopaminergic phenotype. To investigate the impact of aSyn on transcription we infected non-differentiated LUHMES cells with lentivirus encoding for WT aSyn, in a construct expressing GFP using an IRES sequence, or GFP (control cells). Differentiation of LUHMES cells was performed as previously described (32) (Fig 1A). At differentiation day eight, we observed homogeneous GFP-positive cells for both control and WT aSyn expressing cells, that were immunopositive for tyrosine hydroxylase (TH) (Fig 1B). We have recently shown that aSyn expression is distributed throughout the cell, including soma and neurites (32), and induces robust transcription deregulation (32). Here, we investigated the differentially expressed genes further in order to determine major cellular pathways affected by aSyn. Functional enrichment analysis, using both ToppGene Suite software and DAVID, was performed on genes differentially expressed (p-$adj \leq 0.05$, 2167 genes) between control and WT aSyn-expressing cells (Table S1). From these differentially expressed genes, cell cycle was identified as one of the most predominant biological process (ToppGene Suite database identified 349 genes while DAVID detected 195 genes related to cell cycle).

Next, we investigated whether the transcriptional changes were conserved across different cell models. To this end, we performed similar experiments using human H4 neuroglioma cells, a cell model that is more versatile for mechanistic studies of the effect of aSyn in the nucleus. H4 cells express low endogenous levels of aSyn, as detected using conventional protein quantification assays. Immunocytochemistry analysis of H4 cells transiently transfected with WT aSyn showed that the protein was

8

expressed throughout the cell, including the nucleus (Fig 1C). We then performed microarray experiments and identified pathways transcriptionally altered by aSyn. MAS5 analysis detected 3890 genes differentially expressed (p ≤ 0.05) upon aSyn expression (Table S2). As expected, *SNCA*, the gene encoding for aSyn, was up-regulated in WT aSyn H4 cells (ratio=2.02, p=0.01). Functional enrichment analysis, on genes identified with MAS5, showed that aSyn promoted transcriptional changes in several pathways. Consistent with our findings in LUHMES cells, cell cycle was one of the most deregulated biological processes (ToppGene Suite database identified 321 genes related to cell cycle, while DAVID database identified 187 genes) (Table S3).

Interestingly, by comparing the list of genes associated with cell cycle, detected in DAVID analysis, we found 47 genes commonly deregulated upon aSyn expression in both cellular models (Table S4). Nearly 90% of those genes were downregulated (Fig 1D). Protein association network analysis of common genes involved in cell cycle, revealed a strong interaction between these 47 proteins (Fig 1E). CCNB1 showed robust downregulation in both LUHMES and H4 cells, and is extensively connected with most of the other proteins. MKI67, a widely used marker of cell proliferation, and the elongation factor E2F8, were two other genes highly deregulated in both models. The genes encoding these proteins were selected for further validation by qPCR in H4 cells. qPCR analysis confirmed a significant downregulation of *CCNB1* (0.60±0.14 *vs* 1.00±0.06; p=0.0004), *E2F8* (0.73±0.12 *vs* 1.00±0.04; p=0.0011) and *MKI67* (0.65±0.14 *vs* 1.00±0.10; p=0.0019) in H4 cells expressing WT aSyn, compared to control H4 cells (Fig 1F).

Different aSyn species are present in the nucleus

We hypothesized that the impact of aSyn on transcription might be related to its presence in the nucleus. However, the presence of aSyn in the nucleus is still controversial. To clarify this important issue we analysed the subcellular localization of different aSyn species using an array of methodologies. Firstly, we performed immunohistochemistry analyses in brain slices from the temporal lobe of patients with dementia with Lewy bodies (DLB). Using a general anti-aSyn antibody (NCL-L-aSyn) and one against pS129, we observed the occurrence of aSyn and of pS129 aSyn in the nucleus (Fig 2A). We then asked whether aggregated forms of aSyn were detected in the nucleus. Using an antibody specific against aggregated aSyn species (5G4) we also detected immunopositive signals inside the nucleus of cells (Fig 2A). The presence of aggregated aSyn species was further analysed in isolated nuclei derived from the frontal cortex of PD patients. DAPI-positive events (nuclei) were sorted using flow cytometry and additionally separated into NeuN-positive (NeuN+, neuronal) or NeuN-negative (NeuN-, non-neuronal) events (Fig S1A). Extracts from isolated NeuN+ and NeuN- nuclei were resolved in SDS-PAGE and immunobloted with an aSyn oligomer-specific antibody. Three bands were detected in nuclear fractions from both neuronal and non-neuronal samples: a low molecular weight band (~20 kDa) and two bands at ~50 kDa (Fig S1A).

In parallel, we assessed the presence of nuclear aSyn oligomers in H4 cells expressing an aSyn-based bimolecular fluorescence complementary (BiFC) system (Fig S1B), a well-established cell model to study aSyn oligomerization. Using immunocytochemistry (Fig S1C), together with immunoblot analysis of aSyn in nuclear extracts from those cells (Fig S1D), we confirmed that a fraction of aSyn oligomers was present in the nucleus (17.38±3.00 %). We then assessed whether oxidative stress, could modulate the subcellular distribution of aSyn. Treating cells

with 100 μM H_2O_2 for 24h resulted in a significant increase in the levels of aSyn in the nucleus (34.22±6.28 *vs* 17.38±3.00 %; p=0.0138). (Fig S1D).

Additionally, we asked whether the subcellular distribution of aSyn was also affected by the state of differentiation of the cells. For this, we used mouse neuronal stem cells (mNSC) from WT animals. Cells were cultured under maintenance or differentiation conditions, and were immunostained for aSyn and Nestin, a marker of multipotent neuronal stem cells, or aSyn and neuron-specific β-tubulin III (Tuj1) (Fig 2B). Intriguingly, while aSyn was distributed throughout the cytoplasm and nucleus of non-differentiated cells, the protein was mostly located in the nucleus in Tuj-1 positive cells. To confirm this observation, we then performed immunoblot analysis of brain tissue from mice at day 14 of embryonic stage (E14). We observed that ~50% of total aSyn (47.69±5.47 %) was localized in the nuclear fractions (Fig 2C). Interestingly, in the midbrain from young adult mice (2 month-old) only ~18% of the total aSyn (17.43±1.60 %) was nuclear (Fig 2D). As anticipated, immunoblot analysis of midbrain lysates from mice expressing aSyn showed a significant increase in the levels of nuclear aSyn in transgenic mice compared to age-matched WT animals (39.23±7.41 *vs* 17.43±1.60 %; p<0.0076) (Fig 2D).

We also assessed the nuclear content of aSyn in LUHMES and in H4 cells. Consistent with the observations in mice, we found that aSyn was present in the nucleus of control LUHMES cells and also in cells overexpressing aSyn, were the levels of nuclear aSyn were significantly higher (15.19±6.55 *vs* 31.12±3.2 %; p=0.016) (Fig 2E). In H4 cells, aSyn was also detected in the nuclear fraction (8.42±2.63 %) (Fig 2F).

aSyn interacts with DNA, via its N-terminal region, in *in vitro* and *in vivo* PD models

Sporadic reports have suggested that aSyn can interact with DNA, but the domain(s) involved in this binding is/are not known. To investigate aSyn interactions with DNA, we used nuclear magnetic resonance (NMR). First, we found that addition of double stranded DNA induced chemical shift changes in the N- and C-terminus, indicating that aSyn interacts with DNA (Fig 3A). Importantly, the chemical shift perturbations detected in aSyn cannot be attributed to pH or buffer conditions, as no changes were observed for histidine 68, the residue expected to be most sensitive to such effects. Next, we performed similar experiments to investigate whether aSyn could interact with mononucleosomes. Changes in NMR cross peaks were observed for residues at the N-terminus of aSyn, indicating that the N-terminus of the protein interacts with nucleosomes (Fig 3B).

In parallel, we assessed whether aSyn could bind DNA by performing chromatin immunoprecipitation followed by next-generation sequencing (ChIP-seq) experiments in cell and mouse models of PD.

Control and WT aSyn LUHMES cells were cross-linked for ChIP-seq on differentiation day eight. Immunoprecipitation was performed using a monoclonal aSyn antibody, as previously described (11). The sequenced fragments (peaks) were analysed and aligned with the human genome, to allow the identification of genomic regions recruited by endogenous or by overexpressed WT aSyn (Table S5). In this model, ChIP-seq analysis showed binding of endogenous aSyn to genomic regions assigned to 265 unique genes at $p < 0.05$, and 254 genes at $p < 0.01$. A similar number of genes was recruited in cells overexpressing WT aSyn, with 253 genes detected at $p < 0.05$ and 233 at $p < 0.01$. 183 genes ($p < 0.05$) were commonly identified with both

12

endogenous and increased levels of aSyn. In agreement with previous studies, we also identified PGC1-alpha as one of the DNA sites bound by aSyn (11). From the genes that were not bound by aSyn in LUHMES cells expressing WT aSyn, the following showed differential expression in RNA-seq analysis: *ARHGAP15*, *CHFR*, *KCNT2*, *RP11-396K3.1*, *BCL2*, *PCSK5*, *ZNK385D*. From these, *ARHGAP15*, *CHFR*, *KCNT2* and *RP11-396K3.1* were found upregulated, while *BCL2*, *PCSK5* and *ZNK385D* were downregulated.

Motif analysis of ChIP-seq data was performed to ascertain whether there was a specific, consensus binding sequence recognized by aSyn (Table S6). We identified 299 instances in DNA regions interacting with endogenous levels of aSyn, and 87 of those were assigned to promoter regions of 29 genes. In LUHMES cells overexpressing aSyn, 36 out of 178 corresponded to promoter regions assigned to 24 genes. An interesting finding was that detected motifs were enriched in CT sequences. Additional statistical analyses were conducted to differentiate DNA binding of aSyn in control *versus* aSyn overexpressing LUHMES cells (Table S7). Intriguingly, higher expression levels of WT aSyn were associated with lower binding to DNA (Fig 3C). Compared to control LUHMES cells, aSyn in WT aSyn LUHMES cells displayed a significantly ($p<0.01$) lower binding to genomic regions, including regions mapped to centromere (chr21:11,115,832-11,116,620) and telomere (chr2:240,854,721-240,855,315).

To further investigate the biological significance of aSyn binding to DNA, we tested whether changes in aSyn-DNA interactions occurred in a mouse model of PD expressing human WT aSyn, under the Thy-1 promoter. Thus, we performed ChIP-seq experiments using midbrain samples from 6 months old transgenic mice and littermate controls. Our differential analyses of ChIP-seq data generated from these

13

samples (Table S8) confirmed that aSyn is able to bind to several DNA regions, in both WT and transgenic mice. In this model, we also observed that, in the presence of increased WT aSyn levels, aSyn bound significantly less to several genomic regions (p<0.05), corroborating our initial observations in LUHMES cells (Fig 3D). Interestingly, we observed greater binding of mutant A30P aSyn to DNA regions compared to endogenous aSyn (33), highlighting a distinct behavior and cellular impact of both proteins. Furthermore, in control mice, we also detected increased binding of aSyn to DNA sequences near telocentric centromere (chr9: 3,001,360-3,0081,506) and telomeres (i.e. chr17: 92,975,406-92,975,509) (Table S8).

The ability of WT aSyn to interact with DNA was further verified in transfected H4 cells. Analysis of ChIP-seq data confirmed that the ability of aSyn to bind DNA was conserved in this model (Table S9).

Nuclear localization of aSyn is highly dependent on pS129

The translocation of aSyn into the nucleus and the interactions of the protein with nuclear components, such as DNA, may produce alterations in cell homeostasis. Although aSyn lacks an obvious NLS, tagging proteins with such sequences has been widely used to aid in the understanding of the behavior of proteins in specific subcellular compartments. To further investigate the role and biology of aSyn in the nucleus we generated constructs encoding for WT aSyn linked to a nuclear export signal (WT aSyn-NES) or a nuclear localization sequence (WT aSyn-NLS) (Fig 4A). H4 cells transfected with each plasmid expressed increased levels of aSyn, compared to control cells transfected with an empty vector (Fig 4B). The subcellular localization of each aSyn protein was verified by immunostainings in fixed cells (Fig 4C). While WT aSyn exhibited cytoplasmic and nuclear localization, WT aSyn-NES expression

14

was excluded from the nucleus and often accumulated in the perinuclear region (orange arrowhead). Instead, a large fraction of WT aSyn-NLS was localized in the nucleus. Strikingly, in cells transfected with WT aSyn-NLS we observed the formation of nuclear aSyn accumulations or inclusions (green arrowheads). The effect of the NLS on the propensity of the protein for amyloid formation was then analysed using Waltz - an amyloid prediction method (34). This algorithm predicted similar amyloidogenic tendency for both amino acid sequences (Fig S2), suggesting that inclusion formation by WT aSyn-NLS is likely not due to the NLS tag.

Since immunostainings in human brain samples showed presence of pS129 aSyn in the nucleus, we next evaluated the levels of pS129 in H4 cells expressing the various aSyn proteins. pS129 aSyn signal was predominantly distributed in Hoechst-positive regions, indicating that S129 is highly phosphorylated when aSyn is in the nucleus (Fig 4D). At higher magnifications we observed that nuclear accumulations of aSyn in cells transfected with WT aSyn-NLS, also stained positive for pS129, and co-localized with Hoechst-negative nuclear structures, the nucleoli (Fig 4E, green arrow head). Interestingly, we also observed that, in dividing cells, pS129 signal accumulated in structures resembling mitotic spindles (Fig 4E, asterisk and Fig S3A). The localization of aSyn in mitotic spindles was confirmed using two different aSyn antibodies, validating the specificity of the staining (Fig S3B), and was observed throughout different mitotic phases (Fig S3C). While the results from our immunofluorescence experiments show a clear increase in pS129 levels when expressing WT aSyn-NLS, we cannot exclude that these could be a consequence of the increase in the relative concentration of the signal (in the small nucleus vs. spreadout through the cell). To better tackle this question and confirm that nuclear localization of aSyn was associated with increased pS129 levels, we performed

western blotting and quantified pS129 signal relative to total aSyn levels. In cells expressing WT aSyn-NLS the percentage of pS129 was about two-fold higher than for WT aSyn (48.55±20.38 *vs* 17.15±7.70 %; p<0.05) and five-fold higher than WT aSyn-NES (48.55±20.38 *vs* 9.48±8.37 %; p<0.05) (Fig 4F).

Next, to determine whether phosphorylation at Y125 (pY125) could influence the levels of pS129, as previously suggested (35), we performed similar quantifications, using purified pY125 aSyn as a control (Fig 4G). No reactivity was detected in our cell lysates, suggesting that either Y125 phosphorylation was not occurring, or that the levels were below the detection limit of the assay used.

Given the significant increase of pS129 when aSyn was localized in the nucleus, we further investigated the impact of this PTM on nuclear aSyn. For this, we substituted S129 by an alanine (S129A), which cannot be phosphorylated. H4 cells were transfected with either WT aSyn, WT aSyn-NES or WT aSyn-NLS, or with the non-phosphorylatable forms S129A aSyn, S129A aSyn-NES or S129A aSyn-NLS (Fig 5A). Immunoblot analysis of total cell lysates confirmed that no phosphorylation was taking place in the S129A mutants mimicking the unphosphorylated form of aSyn (Fig 5B). The subcellular localization pattern of S129A aSyn-NES was similar to that of WT aSyn-NES (Fig 5C). On the other hand, blocking WT aSyn-NLS S129 phosphorylation increased the cytoplasmic localization of the protein (Fig 5C). To confirm these observations, we performed subcellular fractionation of cells transfected with all aSyn constructs and compared the levels of aSyn in the nucleus of cells expressing the WT aSyn constructs *versus* S129A forms (Fig 5D). Immunoblot quantification showed the following aSyn content (mean ± SD %) in the nucleus: WT aSyn 9.25±2.58 %, S129A aSyn 1.50±1.50 %, WT aSyn-NES 0.98±0.43%, S129A aSyn-NES 1.12±0.72%, WT aSyn-NLS 69.13±1.6%, S129A aSyn-NLS

16

53.55±7.89%. In agreement with our observation in stained cells, significantly lower amounts of aSyn were detected in the nuclear fractions of cells expressing S129A aSyn, when compared to WT aSyn (p=0.0114), and S129A aSyn-NLS, when compared to WT aSyn-NLS (p=0.0286).

To investigate whether the subcellular localization, as well as phosphorylation, interfered with aSyn conformation/oligomerization we analysed cell lysates from transfected cells using non-denaturing conditions (Fig 5E). The pattern of aSyn in native gels showed clear conformational/oligomerization differences between cells expressing aSyn-NES and aSyn-NLS. The apparent molecular weights were consistent with monomeric and small oligomeric forms for WT aSyn and WT aSyn-NES. In contrast, WT aSyn-NLS failed to enter the gel and was stuck in the wells, indicating the protein was aggregating as high molecular weight species (Fig 5E). These results are consistent with our observation that WT aSyn-NLS formed nuclear inclusions. Blocking aSyn S129 phosphorylation did not alter the aggregation of aSyn (Fig 5E).

pS129 modulates aSyn conformation, subcellular localization, and its effect on gene expression

aSyn aggregates are generally characterized by increased content in β-sheet structure and resistance towards proteinase K (PK) digestion. Thus, we next evaluated the sensitivity of aSyn to PK in H4 cells expressing aSyn in different subcellular compartments. Cell lysates were incubated with PK for 5 or 10 minutes. The levels of aSyn at each time point were calculated as relative percentage to the total amount at 0 minutes. Both WT aSyn (69,62±10,30 % at 5 minutes; 44.90±16.41% at 10 minutes) and WT aSyn-NLS (66.32±2.34 % at 5 minutes; 53.60±11.33 % at 10 minutes)

displayed a significantly higher resistance ($p < 0.01$) to PK digestion when compared to WT aSyn-NES (43.88±4.77 % at 5 minutes; 19.31±6.69 % at 10 minutes) (Fig 6A). Interestingly, inhibition of aSyn S129 phosphorylation significantly reduced PK resistance of WT aSyn ($p < 0.001$) and WT aSyn-NES ($p < 0.01$ at 5 minutes; $p < 0.05$ at 10 minutes), while S129A aSyn-NLS was less sensitive to digestion than its WT form ($p < 0.001$ at 5 minutes; $p < 0.05$ at 10 minutes) (Fig 6B), suggesting that phosphorylation may produce differential effects on aSyn depending on the subcellular localization.

Next, we assessed whether the subcellular localization and phosphorylation of aSyn affected its turnover. Cells were treated with cycloheximide (CHX), to inhibit *de novo* protein synthesis, and the levels of aSyn after 12h and 24h of treatment were compared to those before (0h) treatment. Quantification of the immunoblots, 24h after treatment with CHX, revealed that WT aSyn-NLS had a significantly longer half-life compared to WT aSyn (42.08±23.92 *vs* 11.76±0.30 %; $p < 0.05$) and WT aSyn-NES (42.08±23.92 *vs* 9.50±3.50 %; $p < 0.01$) (Fig 6C). Moreover, blocking aSyn S129 phosphorylation only affected the stability of aSyn-NES, since S129A aSyn-NES displayed reduced half-life after 12h treatment, compared to WT aSyn-NES ($p < 0.05$) (Fig 6D).

As described above, expression of WT aSyn promoted severe deregulation of several genes, when comparing with control cells, including downregulation of pivotal genes involved in cell cycle. Next, we asked whether expressing the different aSyn variants would lead to differences in the expression of those genes. We started by assessing gene expression when aSyn was directed to different subcellular compartments. qPCR analysis showed that WT aSyn-NLS cells had significantly increased mRNA levels of *CCNB1*, compared to both WT aSyn (1.49±0.17 *vs* 1.00±0.12; $p < 0.05$) and WT aSyn-

NES cells (1.49±0.17 *vs* 0.88±0.22; p<0.05) (Fig 6E). The levels of *E2F8* and *MKI67* were also significantly upregulated when cells expressed WT aSyn-NLS, but only in comparison to the cells expressing WT aSyn-NES (1.40±0.37 *vs* 0.88±0.14; p<0.05 for *E2F8,* and 1.23±0.32 *vs* 0.87±0.09; p<0.05 for *MKI67*). We next studied the effect of phosphorylation on aSyn-induced transcription deregulation by comparing the expression of these genes when expressing the WT construct and its S129A form. Intriguingly, in H4 cells expressing S129A aSyn-NLS the levels of *CCNB1* and *E2F8* were significantly lower compared to cells expressing WT aSyn-NLS (p=0.0022 for *CCNB1* and p=0.0474 for *E2F8*) (Fig 6F). For *MKI67* a similar trend, that did not reach significance, was observed. The opposite effect was detected when blocking WT aSyn S129 phosphorylation, as S129A aSyn displayed significantly higher mRNA levels of *CCNB1* (p=0.0256) and *E2F8* (p=0.0359). Similarly, compared to its WT form, S129 aSyn-NES showed significantly higher mRNA levels of all three genes (p=0.0019 for *CCNB1*; p<0.0001 for *E2F8* and p=0.0046 for *MKI67*).

The molecular effects induced by nuclear or cytoplasmic aSyn are strongly dependent on S129 phosphorylation

Next, we used an array of assays to dissect the biological impact of aSyn in the nucleus and the role of pS129.

First, we assessed morphological alterations in the Golgi apparatus as an indicator of cellular pathology. H4 cells transfected with various aSyn constructs were co-immunostained for aSyn and Giantin, an endogenous transmembrane protein of the cis and medial Golgi complex (Fig 7A). The number of aSyn expressing cells with normal or fragmented Golgi morphology was determined by fluorescence microscopy and calculated as percentage of total cell number. We found that the percentage of

WT aSyn-NLS cells with fragmented Golgi was significantly lower compared to WT aSyn (38.59±3.76 *vs* 48.43±0.82 %; p<0.05) or WT aSyn-NES (38.59±3.76 *vs* 58.32±3.10 %; p<0.05) (Fig 7B). Moreover, when expressing the WT aSyn-NES a significantly (p<0.05) higher number of cells presented fragmented Golgi (Fig 7B). When comparing each WT aSyn construct with the non-phosphorylatable form (S129A), we found a differential effect of phosphorylation depending on the subcellular localization of the protein (Fig 7C). For WT aSyn we found similar number of cells with normal or fragmented Golgi, while within the population of S129A aSyn expressing cells the percentage of cells with normal Golgi morphology was significantly higher (p<0.05). Likewise, in WT aSyn-NES condition we detected more cells with fragmented Golgi (p<0.05), but no significant difference was detected between the number of cells with normal and fragmented Golgi when S129A aSyn-NES was expressed. In contrast, blocking WT aSyn-NLS S129 phosphorylation (S129A aSyn-NLS) resulted in a significant increase in the percentage of cells with fragmented Golgi (56.82±2.72 *vs* 38.59±3.76 %; p<0.05).

Changes in Golgi morphology are also associated with apoptosis via cleavage of caspase 3 (c-casp3) (36). Thus, we analysed c-casp3, via immunofluorescence, and calculated the number of cells co-expressing aSyn and c-casp3 as a percentage of total aSyn-positive cells. We found that expression of WT aSyn-NES resulted in a significantly greater percentage of aSyn and c-casp3 co-positive cells, compared to cells expressing WT aSyn (170.20±363.84 *vs* 100.00±13.35 %; p<0.05) or WT aSyn-NLS (170.20±363.84 *vs* 59.00±11.90 %; p<0.05) (Fig 7D), which is in agreement with our results on Golgi morphology. We then assessed the impact of phosphorylation on caspase 3 activation and observed that S129A aSyn and S129A aSyn-NES displayed a significant reduction in the percentage of cells immunopositive

20

for c-casp3, when compared to cells expressing WT aSyn (p=0.003) and WT aSyn-NES (p=0.0459), respectively. For cells expressing S129A aSyn-NLS we found a significant increase in apoptosis activation, when compared to WT aSyn-NLS (p=0.0066) (Fig 7E).

Activation of apoptotic signaling cascades may, in some instances, result in increased DNA fragmentation. The impact of aSyn on DNA damage was evaluated via TUNEL and comet assays, in H4 cells expressing the different forms of aSyn. We used these assays as readouts of the molecular effects of aSyn on DNA integrity. The number of TUNEL and aSyn positive cells was calculated as percentage of total amount of aSyn expressing cells. In TUNEL experiments, we observed a significantly higher percentage of fluorescein-positive cells upon WT aSyn-NES expression, compared to WT aSyn cells (137.3±8.68 *vs* 100.0±2.21 %; p<0.05) (Fig 7F). In contrast, WT aSyn-NLS cells displayed a significantly lower percentage of TUNEL-positive cells, compared to both WT aSyn (72.40±11.58 *vs* 100.0±2.21 %; p<0.05) and WT aSyn-NES (72.40±11.58 *vs* 137.3±8.68 %; p<0.05), suggesting that less DNA fragmentation occurs in this condition. In line with Golgi morphology and c-casp3 results, S129A aSyn and S129A aSyn-NES displayed a significantly lower percentage of cells with fragmented DNA when compared with its WT forms (p=0.0305 and p=0.0022, respectively), while inhibiting WT aSyn-NLS S129 phosphorylation (S129A aSyn-NLS) resulted in increased DNA fragmentation (p=0.0280) (Fig 7G).

Similar results were obtained in Comet assay experiments, performed under alkaline conditions. Single comets were visualized by fluorescence microscopy (Fig 7H) and tail moment analysis demonstrated that cells expressing WT aSyn-NES displayed significantly higher tail moments than cells expressing WT aSyn (153.9±34.34 *vs* 100.0±1.40 %; p<0.05) or WT aSyn-NLS (153.9±34.34 *vs* 62.67±22.82 %; p<0.05)

21

(Fig 7I). Blocking S129 phosphorylation resulted in a reduction of tail moment values for both WT aSyn (p=0.0295) and WT aSyn-NES (p=0.0163) (Fig 7J). S129A aSyn-NLS promoted a significant increase of tail moment when compared to its WT form (p=0.0123).

WT aSyn-NES expression also compromised cytoplasmic membrane integrity, as higher levels of adenylase kinase were detected in the supernatant of these cells - compared to both WT aSyn (116.6±9.91 vs 100.0±1.90 %; p<0.05) and WT aSyn-NLS (116.6±9.91 vs 96.13±11.80 %; p<0.05) (Fig 7K). Interestingly, we did not find significant differences between cells expressing WT aSyn and WT aSyn-NLS, suggesting that transcriptional changes may represent an early event in aSyn-induced pathological effects (Fig 7L). Furthermore, S129A aSyn and S129A aSyn-NES were associated with lower toxicity levels when comparing to the respective WT form of aSyn (p=0.002 and p=0.04, respectively). No significant differences were detected in cytoplasmic membrane integrity when aSyn S129 phosphorylation was blocked on WT aSyn-NLS.

To confirm our findings, we infected primary cortical neurons with AAV6 encoding WT aSyn, WT aSyn-NES and WT aSyn-NLS under the synapsin promoter. The subcellular distribution of each aSyn protein was investigated in immunostained neurons, 15 days after viral transduction. We found WT aSyn was present in the soma and in both MAP2-positive neurites (dendrites) and MAP2-negative neuritis (possibly axons) (Fig S4A). In cells expressing WT aSyn-NES, aSyn was present in MAP2-negative neurites and the soma, and was excluded from the nucleus. As expected, WT aSyn-NLS occurred primarily in the nucleus. It has been previously shown that expressing WT aSyn in cortical neurons promotes neurodegeneration (37). Strikingly, both WT aSyn and WT aSyn-NES severely shortened dendritic

arborisation (Fig S4B). In contrast, the dendritic structure was preserved in neurons expressing WT aSyn-NLS, as shown by MAP2 staining.

Discussion

A missing, and rather intriguing, piece in our understanding of aSyn biology is whether the protein occurs physiologically in the nucleus, and whether it may act as a transcriptional modulator upon interacting with nuclear partners. Likewise, little information is available on factors that may modulate the nuclear localization and function of aSyn.

Here, we show that, both in LUHMES and H4 cells, WT aSyn promotes deregulation of several genes. One of the most deregulated pathways in both cell models was cell cycle, suggesting a specific effect on this pathway. We previously reported that both WT and mutant A30P aSyn promote downregulation of genes involved in DNA repair and increased DNA damage (32), two mechanisms that are often associated with cell cycle arrest (38). Interestingly, alterations in cell cycle have been recently linked to neurodegeneration and apoptosis in differentiated cells. In Alzheimer's Disease, abnormal cell cycle re-entry of differentiated neurons is thought to induce apoptosis, since these cells are unable to complete the M-phase (39, 40). Downregulation of initiation and elongation factors are also found in PD patients (12), as well as differential expression of cell cycle genes in PD patients with distinct disease progression (7). Our findings suggest that transcriptional alterations in cell cycle genes might be an important mechanism involved in aSyn pathobiology, but additional studies will be necessary to clarify the relevance of cell cycle disturbances on differentiated neuronal cells, such as LUHMES.

The nuclear localization of aSyn is still controversial, as some studies report lack of aSyn immunoreactivity within the nucleus. One study has shown that discrepancy across studies may be attributable to different specificities of aSyn antibodies (9), but other factors may also lead to such conflicting results. For example, the molecular architecture of the antibodies, which can prevent them from crossing the nuclear envelope, or different structural conformations acquired by aSyn inside the nucleus, due to the interactions with different interacting partners, could lead to different immunoreactivities (41). In fact, using an array of antibodies and molecular techniques, our study provides strong evidence demonstrating the occurrence of different aSyn species in cell nucleus. These findings are consistent with previous reports showing different aSyn species inside the nuclei of neuronal cells from PD patients (11, 12), in mouse and cellular models of the disease (11, 14-16). Curiously, in patients with Multiple Systems Atrophy, nuclear aSyn inclusions are also observed in oligodendrocytes (42). In agreement with other reports (11, 43, 44) we have detected higher amounts of aSyn oligomers in the nucleus of stressed cells, which is in line with an active intracellular dynamics between nuclear and cytoplasmic localization (23). A preferential nuclear localization of aSyn in maturing neurons of the *substantia nigra* (45) and in developing mice (16) has been also sporadically reported. Here we have also found a strong nuclear presence of aSyn in differentiating mNSC and E14 mice. These results suggest that under physiological conditions, aSyn may play a role in the nucleus to ensure the correct differentiation and/or division of cells, possibly by acting as a transcriptional modulator. Importantly, it has been suggested that nuclear aSyn is involved in the initiation of DNA replication, by maintaining Mcm proteins in the chromatin (18).

24

Our findings highlight the need for understanding the mechanisms underlying aSyn-induced transcriptional deregulation and the biological significance of nuclear aSyn. An attractive hypothesis is that aSyn disrupts transcription via interactions with DNA. Binding of aSyn to DNA was previously reported (11, 25, 46) and we have recently shown binding of A30P aSyn (33). However the domains of aSyn that interact with DNA are not known. In the presence of a small DNA sequence, we observed structural alterations in both the N- and C-termini. As the interaction of aSyn with DNA is likely to be electrostatic, one can speculate that the interaction occurs via positively charged residues at the N-terminus, while the NMR signal shifts in the C-terminus may indicate changes in the ensemble conformations, due to repulsion between the DNA bound to the N-terminus and the negatively charged C-terminus. Furthermore, when incubating aSyn with nucleosomes a distinct interaction was detected between DNA and the N-terminus of the protein, suggesting the interaction is context-dependent.

In agreement with previous studies (11, 25), results from ChIP-seq experiments showed that aSyn binds several DNA regions in mice and cellular models of PD. Motif analysis on ChIP-seq hits revealed that aSyn preferentially interacts with DNA regions rich in CT/GA nucleotides, while previous *in vitro* studies suggested a preferential interaction with GC-box-like sequences (47). Intriguingly, we found that increased expression of aSyn in LUHMES cells resulted in a reduction in the DNA regions immunoprecipitated. These results were further confirmed in a transgenic mouse model expressing human aSyn. Interestingly, we have observed greater binding of A30P aSyn to DNA, in the same model (33). In 6 month-old mice, greater A30P aSyn-DNA binding produced a robust deregulation in the expression of several genes involved in ER-Golgi system, while in WT aSyn mice only 18 genes were

found deregulated (33). These results highlight the differential impact of these proteins in distinct cellular processes and suggest that alterations in WT aSyn-DNA interactions as a potentially relevant event in early stages of PD pathophysiology. Although we cannot precisely define the mechanisms underlying the reduction of aSyn binding to DNA, it is possible that, in pathological conditions, changes in aSyn conformation, for example due to PTMs or aggregation, may alter its ability to bind DNA, leading to reduced binding from important DNA regions and to consequent alterations in DNA integrity and gene expression. Reduction in DNA binding was particularly significant in centromeric and telomeric regions, two regions involved in DNA stability. Interestingly, a recent study showed that telomere shortening accelerates aSyn pathology (48). Overall, we speculate that under pathological conditions aSyn may detach from important DNA regions, altering DNA integrity and gene expression. Interestingly, a similar behavior was suggested for the neurodegeneration-associated protein Tau (49), suggesting that protein-DNA interactions may have been overlooked and may play an underappreciated role in neurodegeneration.

To gain further insight into the biochemical effect of aSyn in the nucleus, we compared two extreme situations where aSyn was primarily present in the cytoplasm (WT aSyn-NES) or in the nucleus (WT aSyn-NLS). We found that WT aSyn-NLS was strongly phosphorylated at S129 and was associated with the formation of high molecular weight nuclear inclusions that were excluded from the nucleoli, as we have previously reported in primary cell cultures treated with exogenous, recombinant aSyn (21). WT aSyn and WT aSyn-NLS displayed increased resistance to PK digestion, when compared with WT aSyn-NES, indicating that the conformation of aSyn may depend on its subcellular localization. However, we cannot completely

exclude that differential PK resistance may also be due to the presence of NLS and NES.

The few studies available on the toxicity associated with the presence of aSyn in the nucleus are contradictory. Most report increased (11, 14, 19), while others report reduced neurotoxicity (18, 21), demonstrating our lack of understanding of the process. One report also suggests that the protein may play a dual role in the nucleus, shifting between a protective or toxic function in response to specific stress condition or molecular factors (18). Our study provides new insight into this important topic, showing that aSyn conformation and phosphorylation status on S129 may be important modulators of the effects of aSyn on gene expression and overall cellular homeostasis. We found that in cells expressing higher amounts of aSyn in the nucleus (WT aSyn-NLS), and containing high molecular weight aSyn species, the levels of *CCNB1*, *E2F8* and *MKI67* were upregulated, when compared to cells expressing WT aSyn. Importantly, transcriptional alterations induced by WT aSyn-NLS were concomitant with reduced cell damage and pathological effects, in both H4 cells and primary cortical neurons. In contrast, expression of WT aSyn or WT aSyn-NES promoted caspase 3 activation, increased DNA damage and cellular toxicity. We also found that aSyn S129 phosphorylation may be pivotal for the nuclear localization of the protein, and may modulate its toxicity and effect on transcription on a localization-dependent manner. Compared to WT aSyn-NLS, S129A aSyn-NLS exhibited lower nuclear localization, promoted downregulation of *CCNB1*, *E2F8* and increased cell damage. Nevertheless, and although the S129A substitution has been widely used to block aSyn phosphorylation, we cannot fully exclude the possibility that a slight difference in the amount of nuclear aSyn observed when expressing S129A-NLS compared to WT-NLS may be due to an effect of the mutation, and not

just due to a change in the phosphorylation status. Since S129 phosphorylation is known to affect aSyn protein-protein interactions (28), we hypothesized that structural changes promoted by blocking WT aSyn-NLS S129 phosphorylation, such as enrichment for β-sheets structures, might promote erroneous interactions between aSyn and nuclear factors, leading to DNA instability and transcription deregulation. Intriguingly, we found that inhibition of WT aSyn or WT aSyn-NES S129 phosphorylation resulted in the up-regulation of cell cycle genes and lower toxicity, an effect that might be mediated by the sequestration or lack of sequestration of transcription factors in the cytoplasm.

Several reasons may explain the discrepancies between our results and previous findings showing an association between the presence of aSyn in the nucleus and increased toxicity (e.g. trivial differences such as the use of different constructs). Nevertheless, our findings are consistent with our interpretation that PTMs, such as pS129, and the type of aSyn species may determine its effect in the nucleus. Additionally, since aSyn toxicity is known to be dose-dependent, one cannot exclude that even subtle expression differences between experiments may affect the outcome. Importantly, we have previously demonstrated that aggregated, highly pS129 nuclear aSyn is not associated with increased toxicity in primary cell cultures (21). Likewise, in Huntington's disease, nuclear huntingtin inclusions were also demonstrated to be protective (50).

Overall we hypothesize that, under physiological conditions, the interplay between aSyn nuclear localization, phosphorylation and transcription regulation via binding to DNA may play an important role in cell homeostasis, cell division, and differentiation (Fig S5 A-F). However, increased levels of aSyn that may result in the accumulation of non-phosphorylated high molecular weight aSyn species inside the nucleus, may

reduce its binding to DNA and enhance toxicity by inducing severe transcriptional deregulation, such as downregulation of important cell cycle genes (Fig S5 G-Q). Although our findings provide novel insights into the role of aSyn in the nucleus, future studies will be necessary to clarify the link between deregulation of cell cycle and toxicity, and the impact of modulating the expression of those genes on cellular homeostasis. While the use of aSyn constructs is helpful to investigate the behavior of the protein in different subcellular locations, it will also be important to modulate aSyn phosphorylation by using specific kinases to understand the physiological impact of this posttranslational modification on the subcellular localization of aSyn and on its effect on transcription. Furthermore, in our study, we have only addressed the effect of one posttranslational modification on the subcellular dynamics of aSyn. However, aSyn is known to undergo several other modifications that are thought to form a complex crosstalk (51). It is also important to note that our findings raises the question on whether loss of DNA binding is specifically caused by higher levels of aSyn or is rather a consequence of aSyn aggregation upon increasing the levels of the protein. This should be further investigated in future studies. Thus, additional studies will be instrumental in order to provide detailed understanding of the biology of aSyn, such as its subcellular distribution, and effects on gene expression. Ultimately, this information will be essential for the development of novel strategies for intervention in PD and other synucleinopathies.

Materials and Methods

Cell culture

Mouse neural stem cells (mNSC)

Primary mNSCs were isolated from single WT mouse brains at E12.5-E14.5. mNSCs were cultured and differentiated as described before (52). mNSCs were kept under differentiation for 5 days and then seeded onto coverslips for immunostainings.

LUHMES cells

LUHMES cells were a kind gift from Prof. Marcel Leist and were cultured and differentiated as previously described(32). Experiments were performed eight days after differentiation.

Human neuroglioma (H4) cells

Cells were cultured in Dulbecco's Modified Eagle Medium (DMEM, Life Tecnologies-Invitrogen, Carlsbad, CA, USA) supplemented with 10% fetal bovine serum (FBS, PAA, Cölbe, Germany) and 1% Penicillin-Streptomycin (PS). H4 cells were grown at 37ºC in humidified 5% CO_2 atmosphere.

H4 cells expressing the BiFC system

Yellow fluorescence protein reconstitution assay was made as previously described for green fluorescence protein (15). H4 cells stability expressing the two aSyn-Venus BiFC plasmids, VN-aSyn and aSyn-VC, were used. Cells were cultured in DMEM with 10% FCS, 1% PS and 250 μg/mL geneticin (G418, Invivogen).

Primary cultures

Primary cortical cultures were prepared from rat pups at E18, as previously described (53). Cells were seeded in PLO pre-coated glass coverslips and were grown in Neurobasal medium (Gibco), supplemented with 1% Pencillin-Streptomycin (Pan-Biotech), 0.5 mg/mL Transferrin (Sigma), 125mM L-glutamine (Pan-Biotech) and 1x B27 (Gibco), at 37ºC in humidified 5% CO_2 atmosphere.

Generation of LUHMES cells expressing WT aSyn

Control LUHMES cells and LUHMES cells expressing WT aSyn were generated using lentiviral vectors, as previously described (32).

Generation of aSyn constructs

The original plasmids used as template for the generation of WT aSyn-NES and WT aSyn-NLS were kindly provided by Prof. Dr. Poul Henning Jensen (Aarhus University, Denmark). To express aSyn solely in the cytoplasm or in the nucleus aSyn was tagged with a nuclear export sequence (NES) or a nuclear localization sequence (NLS), respectively. To obtain aSyn constructs that could not be phosphorylated at serine 129, we performed site-directed mutagenesis in all abovementioned plasmids (WT aSyn, WT aSyn-NES and WT aSyn-NLS) to substitute the serine residue at position 129 by an alanine (S129A aSyn, S129A aSyn-NES and S129A aSyn-NLS), using the QuickChange II Site-Directed Mutagenesis Kit (Agilent Tecnhologies, SC, USA).

Transfection of H4 cells

H4 cells were seeded in different well-plate formats (Costar, Corning, NY, USA), at proper density, 24h prior to transfection with Calcium Phosphate. Transfections were

31

performed as previously described (54). Unless otherwise stated, experiments were performed 48h after transfection.

Generation of AAV6 for infecting primary cell cultures

cDNA encoding for WT aSyn, WT aSyn-NES and WT aSyn-NLS were subcloned into an AVV vector genome with AAV-2 ITRs, under the synapsin promoter. Recombinant virus was packaged into AAV-6 capsids as previously described (55). Neuronal cells were infected at day *in vitro* 3 with equimolar amounts of AAV-6 WT aSyn, WT aSyn-NES or WT aSyn-NLS (1.10^8 vg/well). 15 days after transduction, cells were processed for immunocytochemistry analysis.

Immunocytochemistry – cell culture

For immunofluorescence microscopy cells were fixed, permeabilized with 0.5% Triton/PBS, and blocked with 3% BSA/PBS. Primary antibodies, diluted in blocking solution, were incubated overnight at 4ºC. Secondary Alexa Fluor antibodies diluted 1:1000, in blocking buffer, were incubated for 2 hours, at RT. Nuclei were stained with Hoechst. Images were acquired using an epifluorescence microscope (Leica DMI 6000B microscope, Leica). Immunostainings were performed in cells derived from three independent differentiations (LUHMES cells), transfections (H4 cells) or preparations (primary neuronal cells).

Human brain tissue

Brain tissue from a DLB case was obtained from Newcastle Brain Tissue Resource (NBTR) in accordance with the approval of the joint Ethics Committee of Newcastle and North Tyneside Health Authority and following NBTR brain banking procedures.

Samples of brain tissue from PD patients were obtained from the Institute of Neuropathology HUB-ICO-IDIBELL Biobank and the Hospital Clinic-IDIBAPS Biobank following the Spanish legislation procedures and upon approval of the local ethics committees. Samples of frontal cortex area 8 from PD patients were obtained from the Institute of Neuropathology HUB-ICO-IDIBELL Biobank following the Spanish legislation procedures and upon approval of the local ethics committee. For this study, 2 PD cases stages 5–6 aged 72 and 74 years were analyzed (12).

Immunohistochemistry on DLB tissue

At autopsy, the right hemisphere immersed in 4% buffered aqueous formaldehyde, fixed for 4 to 6 weeks, processed to paraffin wax and underwent standardised neuropathological assessment according to internationally recognised criteria (56). Sections were immunostained for antibodies against three aSyn epitopes (anti-p-aSyn, anti-NCL-L-aSyn and anti-5G4). Immunopositivity was detected using a MENAPATH HRP polymer detection kit (Menarini diagnostics) with 3,3 diaminobezidine (DAB) and haematoxylin. Stained sections were assessed for presence of aSyn in the nucleus at x600 magnification, using a NIS Eclipse 90i microscope and DsFi1 camera (Nikon, Surry, UK).

TUNEL assay

Deoxynucleotidyl transferase dUTP nick end-labeling assay (TUNEL, *In Situ* Cell Death Detection Kit, Roche) was used according to the manufacturer's instructions, after immunostainning cells for aSyn. Detection and quantification of aSyn and TUNEL-labeled cells was performed via an automated fluorescence microscope system.

Golgi fragmentation

H4 cells were immunostained for aSyn and Giantin. Immunofluorescence images were randomly acquired using an epifluorescence microscope (Leica DMI 6000B microscope, Leica). Cells were classified according to its Golgi morphology, as either normal or fragmented.

Immunoblots

At indicated time points, cells were harvest in RIPA, sonicated and centrifuged. Bradford assay (BioRad, USA) was used to assess protein concentration. 40-60 μg of total lysate was mixed with 5x Laemmli buffer and boiled at 95ºC for 5 minutes. Samples were electrophoresed through 12% sodium dodecyl sulfate polyacrylamide (SDS-PAGE) gels and transferred to nitrocelulose membranes (Trans-blot Turbo Nitrocellulose membranes, BioRad). After blocking, primary antibodies diluted in blocking solution were incubated overnight, at 4ºC. Membranes were then incubated with either horseradish peroxidase-conjugated secondary antibodies (GE Healthcare), or IRDye secondary antibodies, for 2h, at RT. Chemiluminescent signals on the blots were detected using Immobilon Western Chemiluminescent HRP Substrate (Millipore Corporation, USA) and Fusion FX (Vilber Lourmat, France), while fluorescent signals were visualized using Odyssey CLx (Licor). Quantification of bands was performed using Image J software.

Nuclei isolation from cells obtained from PD patients

Nuclei isolation was performed as previously described (12). Isolated nuclei werestained with NeuN antibody. Upon incubation with secondary antibody Alexa

488, DNA content was labeled with DAPI. Nuclei were sorted via flow cytometry, in a Beckman Coulter MoFlo Astrios. NeuN+ and NeuN- nuclei were collected in Optiprep and centrifuged at 3,2000f for 20 minutes at 4ºC. Obtained pellet were mixed with Laemmli and resolved in 10% SDS-PAGE.

Half-life measurements

To determining the half-life of each aSyn constructs used in this study transfected cells were treated with cycloheximide (CHX, Sigma) 24h after transfection. Lysates from non-treated cells, or cells treated with 150 μM CHX for 12h or 24h were harvested at the same time and analysed on SDS-PAGE gel.

Proteinase K digestion

Transfected cells were incubated with 1% TritonX-100/PBS, on ice, for 30 minutes, sonicated and digested with 10 μg/mL of freshly prepared Proteinase K, for different periods (0, 5 and 10 minutes). Afterwards, lysates were mixed with 5x Laemmli buffer, boiled at 95ºC for 5 minutes, electrophoresed on 12% SDS-PAGE gels and immunobloted.

Subcellular fractionation of cells

To separate cytoplasmic and nuclear fractions, cells were incubated with a weak lysis buffer. Following centrifugation, the cytoplasmic fraction was recovered. Nuclear pellet was washed was then resuspended in buffer. After centrifugation, supernatant (nuclear fraction) was recovered.

Subcellular fractionation of mice brain

Animals were housed and handled according to institutional and national guidelines. Whole brains from E14 pulps were isolated from WT mice. In parallel, midbrain of 2 month old WT and transgenic mice *mus musculus*, C57BL/6xDBA, males) overexpressing WT aSyn, under the Thy-1 promoter (57), were dissected. Collected tissues were homogenized with a weak lysis buffer and, following centrifugation, supernatant (cytoplasmic fractions) were stored. Nuclear pellet were then homogenized with lysis buffer and nuclear fractions were obtained upon centrifugation.

Native PAGE

For native gel electrophoresis samples were lysated in detergent-free lysis buffer [0,8% TritonX in 50 mM Tris, pH 7.40, 0.15 M NaCl and Protease Inhibitor Cocktail (Roche)]. Samples were mixed with protein sample buffer (5x: 0.31 M Tris HCl pH 6.8, Glycerol 50%, 0,4% Bromophenol blue), loaded on precast vertical Serva gels 4-16% (Serva) and ran on 1x running buffers from Serva [Anode (50 mM BisTris-HCl pH 7.0), Cathode (50 mM Tricin, 15 mM BisTris-HCl pH 7.0)].

Comet assay

Comet assay experiments were performed as previously described(32), under alkaline conditions. Slides were stained with 2.5 µg/mL of propidium iodide and analysed using an epifluorescence microscope (Leica DMI 6000B microscope, Leica). Tail moments were calculated using the Comet Score software.

Toxicity Measurements

36

ToxiLight BioAssay kit (Lonza) was used, according to the manufacture recommendations, and luminescence was measured with an Infinite M2000 PRO plate reader (Tecan Lta, Switzerland).

NMR spectroscopy

WT aSyn was expressed in Escherichia coli BL21 using a pT7-7 plasmid encoding for the human protein. Protein expression and purification was performed as previously described (58). Purified aSyn was labelled with ^{15}N by using M9-minimal medium supplemented with ^{15}NH$_4$Cl (Cambridge Isotope Laboratories). Nucleosomes were assembled on 200 bp 601 sequence DNA and using recombinant *Xenopus laevis* core histones.

NMR experiments were performed with samples containing 50 μM of labelled WT aSyn and either 70 μM annealed complementary primers of 30 bases or nucleosomes, in 50 mM HEPES buffer, 100 mM NaCl, pH 7.4. Data was recorded using a Bruker Avance 600 MHz spectrometer. Data processing was performed using the software packages Topspin (Bruker) and CCPN Analysis (59).

ChIP-seq experiments

Sample collection

Samples from transgenic mice, LUHMES and H4 cells were collected and processed for ChIP-seq analysis. Half midbrains of 6 months old transgenic and control mice were dissected and cut cut in ~1 mm^3 pieces. Tissue from mice, LUHMES cells, and H4 cells were cross-linked, pelleted and lysed.

Chromatin shearing and library preparation

Chromatin was sheared using a Diagenode Bioruptor sonicator and fragment sizes were checked. Prior to chromatin pre-clearing, a fraction of the chromatin was aliquoted as total input (Input). Chromatin immunoprecipitation (IP) was performed using 4 µg of monoclonal aSyn antibody for mouse and LUHMES samples, and anti-myc antibody for H4 samples. Precipitated chromatin was eluted and, after reversing the crosslinks, DNA was purified with QIAquick PCR Purification Kit (Qiagen) and quantified using PicoGreen or NanoDrop Spectrophometer for IP and Input DNA, respectively. Library preparation of all IP and Input samples were performed with TruSeq ChIP Library preparation kit (Illumina) and checked using Agilent Bioanalyzer HS DNA kit. High-throughput sequencing of those fragments of LUHMES samples was performed with Illumina Genome Analyzer IIX. Mice samples were sequenced using MiSeq (Illumina).

ChIP-seq analysis

Mice samples were aligned to UCSC mm10 using BaseSpace Sequence Hub (Illumina). ELAND software (Illumina) was used to align all reads of LUHMES to the repeat masked NCBI 36/hg18 build of the human genome, allowing up to two mismatches. The Partek Genomics Suite (Partek) ChIP-seq analysis workflow was used to identify enriched aSyn binding region of aSyn. Peaks were determined using a 100 bp window and the zero-truncated binomial model with a peak cut-off p-value of 0.001. Additionally, ChIP-seq samples from transgenic mice and LUHMES cells were subjected to differential binding analysis using DiffBind package of Bioconductor (60) with an in-built option of DESEQ2 (61). For the analysis with Diffbind peaks were called with MACS2 (62) using the q-value of 0.1 ("q 0.1" option).

Gene expression studies

<u>RNA isolation</u>

Total RNA was extracted and reversed-transcribed using the RNeasy mini kit (Qiagen, Germany) and the QuantiTect Reverse Transcription kit (Qiagen, Germany), respectively, following the protocol provided by the manufactures.

<u>Gene expression analysis through RNA-seq</u>

Sequencing and differential gene expression analysis on LUHMES cells was performed as previously described (32).

<u>Microarray analysis</u>

RNA was isolated from H4 control cells and WT aSyn expressing H4 cells (myc-tagged) using the RNeasy kit (Qiagen) according to the manufacturer's instructions. RNA was processed using the standard One-Cycle cDNA Synthesis Affymetrix protocol and Human Genome U133 PLUS 2.0 arrays, containing 54,675 25-mer probes, was used for gene expression profiling.. Feature extraction, normalization and calculation of signal values were performed using the MAS software algorithm.

<u>Functional enrichment analysis</u>

Gene ontology analysis on differentiated genes was performed using the bioinformatics tool ToppGene Suite and through DAVID. STRING online software was used for network analysis of cell cycle-related genes.

<u>Data Availability</u>

All expression data files are available in the GEO database (GEO Series accession number GSE89115). Microarray data generated from H4 cells has been also submitted to the GEO database (GSE95427).

Real-time PCR

Total RNA was extracted and reversed-transcribed using the RNeasy mini kit (Qiagen, Germany) and the QuantiTect Reverse Transcription kit (Qiagen, Germany), respectively, following the protocol provided by the manufactures. qPCRs were prepared according to the Mesa Blue qPCR MasterMix Plus for SYBR Assay (Eurogentec, Belgium) instructions, and were carried out in a a Mx300P cycler (Agilent Techonolgy, USA). Relative quantification of genes of interest was calculated using the Ct values obtained via MxPro software. To determine fold-change expressions the 2-ΔΔCt method was used (63). Briefly, ΔCt was calculated by substracting the Ct value from targeted genes to the Ct value of B-actin. ΔCt of the control sample was subsequently subtracted by the ΔCt of each tested condition to obtain ΔΔCt. Fold change were calculated using the formula 2-ΔΔCt. Graphs show relative 2-ativ values compared to control or WT aSyn.

Statistical analysis

Data in graphs are presented as mean ± SD. Each N represents one independent experiment. When replicates were performed in one N, the average of the replicates was considered. Significance of differences was calculated in GraphPad Prism 5 software (California, USA), using Unpaired t-test to compare two groups and one-

way or two-way ANOVA for multiple comparisons. p<0.05 was considered to indicate a significant difference.

Acknowledgements

Conflict of Interest Statement

The authors declare no conflict of interests.

References

1   Polymeropoulos, M.H., Lavedan, C., Leroy, E., Ide, S.E., Dehejia, A., Dutra, A., Pike, B., Root, H., Rubenstein, J., Boyer, R. *et al.* (1997) Mutation in the alpha-synuclein gene identified in families with Parkinson's disease. *Science*, **276**, 2045-2047.

2   Simon-Sanchez, J., Schulte, C., Bras, J.M., Sharma, M., Gibbs, J.R., Berg, D., Paisan-Ruiz, C., Lichtner, P., Scholz, S.W., Hernandez, D.G. *et al.* (2009) Genome-wide association study reveals genetic risk underlying Parkinson's disease. *Nat. Genet.*, **41**, 1308-1312.

3   Spillantini, M.G., Schmidt, M.L., Lee, V.M., Trojanowski, J.Q., Jakes, R. and Goedert, M. (1997) Alpha-synuclein in Lewy bodies. *Nature*, **388**, 839-840.

4   Yacoubian, T.A., Cantuti-Castelvetri, I., Bouzou, B., Asteris, G., McLean, P.J., Hyman, B.T. and Standaert, D.G. (2008) Transcriptional dysregulation in a transgenic model of Parkinson disease. *Neurobiology of disease*, **29**, 515-528.

5   Miller, R.M., Kiser, G.L., Kaysser-Kranich, T., Casaceli, C., Colla, E., Lee, M.K., Palaniappan, C. and Federoff, H.J. (2007) Wild-type and mutant alpha-synuclein induce a multi-component gene expression profile consistent with shared pathophysiology in different transgenic mouse models of PD. *Experimental neurology*, **204**, 421-432.

6   Grunblatt, E., Mandel, S., Jacob-Hirsch, J., Zeligson, S., Amariglo, N., Rechavi, G., Li, J., Ravid, R., Roggendorf, W., Riederer, P. *et al.* (2004) Gene expression profiling of parkinsonian substantia nigra pars compacta; alterations in ubiquitin-proteasome, heat shock protein, iron and oxidative stress regulated proteins, cell adhesion/cellular matrix and vesicle trafficking genes. *Journal of neural transmission*, **111**, 1543-1573.

7   Pinho, R., Guedes, L.C., Soreq, L., Lobo, P.P., Mestre, T., Coelho, M., Rosa, M.M., Goncalves, N., Wales, P., Mendes, T. *et al.* (2016) Gene Expression Differences in Peripheral Blood of Parkinson's Disease Patients with Distinct Progression Profiles. *PloS one*, **11**, e0157852.

8   Soreq, L., Ben-Shaul, Y., Israel, Z., Bergman, H. and Soreq, H. (2012) Meta-analysis of genetic and environmental Parkinson's disease models reveals a common role of mitochondrial protection pathways. *Neurobiology of disease*, **45**, 1018-1030.

9   Huang, Z., Xu, Z., Wu, Y. and Zhou, Y. (2011) Determining nuclear localization of alpha-synuclein in mouse brains. *Neuroscience*, **199**, 318-332.

10   Wales, P., Pinho, R., Lazaro, D.F. and Outeiro, T.F. (2013) Limelight on alpha-synuclein: pathological and mechanistic implications in neurodegeneration. *Journal of Parkinson's disease*, **3**, 415-459.

11   Siddiqui, A., Chinta, S.J., Mallajosyula, J.K., Rajagopolan, S., Hanson, I., Rane, A., Melov, S. and Andersen, J.K. (2012) Selective binding of nuclear alpha-synuclein to the PGC1alpha promoter under conditions of oxidative stress may contribute to losses in mitochondrial function: implications for Parkinson's disease. *Free Radic. Biol. Med.*, **53**, 993-1003.

12   Garcia-Esparcia, P., Hernandez-Ortega, K., Koneti, A., Gil, L., Delgado-Morales, R., Castano, E., Carmona, M. and Ferrer, I. (2015) Altered machinery of protein synthesis is region- and stage-dependent and is associated with alpha-synuclein oligomers in Parkinson's disease. *Acta neuropathologica communications*, **3**, 76.

13   Maroteaux, L., Campanelli, J.T. and Scheller, R.H. (1988) Synuclein: a neuron-specific protein localized to the nucleus and presynaptic nerve terminal. *J Neurosci*, **8**, 2804-2815.

14   Kontopoulos, E., Parvin, J.D. and Feany, M.B. (2006) Alpha-synuclein acts in the nucleus to inhibit histone acetylation and promote neurotoxicity. *Hum. Mol. Genet.*, **15**, 3012-3023.

15   Outeiro, T.F., Putcha, P., Tetzlaff, J.E., Spoelgen, R., Koker, M., Carvalho, F., Hyman, B.T. and McLean, P.J. (2008) Formation of toxic oligomeric alpha-synuclein species in living cells. *PloS one*, **3**, e1867.

43

16   Zhong, S.C., Luo, X., Chen, X.S., Cai, Q.Y., Liu, J., Chen, X.H. and Yao, Z.X. (2010) Expression and subcellular location of alpha-synuclein during mouse-embryonic development. *Cell. Mol. Neurobiol.*, **30**, 469-482.

17   Goers, J., Manning-Bog, A.B., McCormack, A.L., Millett, I.S., Doniach, S., Di Monte, D.A., Uversky, V.N. and Fink, A.L. (2003) Nuclear localization of alpha-synuclein and its interaction with histones. *Biochemistry*, **42**, 8465-8471.

18   Liu, X., Lee, Y.J., Liou, L.C., Ren, Q., Zhang, Z., Wang, S. and Witt, S.N. (2011) Alpha-synuclein functions in the nucleus to protect against hydroxyurea-induced replication stress in yeast. *Hum. Mol. Genet.*, **20**, 3401-3414.

19   Ma, K.L., Song, L.K., Yuan, Y.H., Zhang, Y., Han, N., Gao, K. and Chen, N.H. (2014) The nuclear accumulation of alpha-synuclein is mediated by importin alpha and promotes neurotoxicity by accelerating the cell cycle. *Neuropharmacology*, **82**, 132-142.

20   Schell, H., Hasegawa, T., Neumann, M. and Kahle, P.J. (2009) Nuclear and neuritic distribution of serine-129 phosphorylated alpha-synuclein in transgenic mice. *Neuroscience*, **160**, 796-804.

21   Villar-Pique, A., Lopes da Fonseca, T., Sant'Anna, R., Szego, E.M., Fonseca-Ornelas, L., Pinho, R., Carija, A., Gerhardt, E., Masaracchia, C., Abad Gonzalez, E. *et al.* (2016) Environmental and genetic factors support the dissociation between alpha-synuclein aggregation and toxicity. *Proceedings of the National Academy of Sciences of the United States of America*, **113**, E6506-E6515.

22   Wakamatsu, M., Ishii, A., Ukai, Y., Sakagami, J., Iwata, S., Ono, M., Matsumoto, K., Nakamura, A., Tada, N., Kobayashi, K. *et al.* (2007) Accumulation of phosphorylated alpha-synuclein in dopaminergic neurons of transgenic mice that express human alpha-synuclein. *Journal of neuroscience research*, **85**, 1819-1825.

23   Goncalves, S. and Outeiro, T.F. (2013) Assessing the subcellular dynamics of alpha-synuclein using photoactivation microscopy. *Molecular neurobiology*, **47**, 1081-1092.

24   Azeredo da Silveira, S., Schneider, B.L., Cifuentes-Diaz, C., Sage, D., Abbas-Terki, T., Iwatsubo, T., Unser, M. and Aebischer, P. (2009) Phosphorylation does not prompt, nor prevent, the formation of alpha-synuclein toxic species in a rat model of Parkinson's disease. *Hum. Mol. Genet.*, **18**, 872-887.

25   Martins, M., Rosa, A., Guedes, L.C., Fonseca, B.V., Gotovac, K., Violante, S., Mestre, T., Coelho, M., Rosa, M.M., Martin, E.R. *et al.* (2011) Convergence of miRNA expression profiling, alpha-synuclein interacton and GWAS in Parkinson's disease. *PloS one*, **6**, e25443.

26   Cherny, D., Hoyer, W., Subramaniam, V. and Jovin, T.M. (2004) Double-stranded DNA stimulates the fibrillation of alpha-synuclein in vitro and is associated with the mature fibrils: an electron microscopy study. *Journal of molecular biology*, **344**, 929-938.

27   Jiang, P., Gan, M., Yen, S.H., Moussaud, S., McLean, P.J. and Dickson, D.W. (2016) Proaggregant nuclear factor(s) trigger rapid formation of alpha-synuclein aggregates in apoptotic neurons. *Acta neuropathologica*, **132**, 77-91.

28   Oueslati, A. (2016) Implication of Alpha-Synuclein Phosphorylation at S129 in Synucleinopathies: What Have We Learned in the Last Decade? *Journal of Parkinson's disease*, **6**, 39-51.

29   Basso, E., Antas, P., Marijanovic, Z., Goncalves, S., Tenreiro, S. and Outeiro, T.F. (2013) PLK2 modulates alpha-synuclein aggregation in yeast and mammalian cells. *Molecular neurobiology*, **48**, 854-862.

30   Tenreiro, S., Reimao-Pinto, M.M., Antas, P., Rino, J., Wawrzycka, D., Macedo, D., Rosado-Ramos, R., Amen, T., Waiss, M., Magalhaes, F. *et al.* (2014) Phosphorylation modulates clearance of alpha-synuclein inclusions in a yeast model of Parkinson's disease. *PLoS genetics*, **10**, e1004302.

31   Tenreiro, S., Eckermann, K. and Outeiro, T.F. (2014) Protein phosphorylation in neurodegeneration: friend or foe? *Frontiers in molecular neuroscience*, **7**, 42.

32   Paiva, I., Pinho, R., Pavlou, M.A., Hennion, M., Wales, P., Schutz, A.L., Rajput, A., Szego, E.M., Kerimoglu, C., Gerhardt, E. *et al.* (2017) Sodium butyrate rescues dopaminergic cells from alpha-synuclein-induced transcriptional deregulation and DNA damage. *Hum. Mol. Genet.*, **26**, 2231-2246.

33   Paiva, I., Jain, G., Lazaro, D.F., Jercic, K.G., Hentrich, T., Kerimoglu, C., Pinho, R., Szego, E.M., Burkhardt, S., Capece, V. *et al.* (2018) Alpha-synuclein deregulates the expression of COL4A2 and impairs ER-Golgi function. *Neurobiology of disease*, **119**, 121-135.

34   Maurer-Stroh, S., Debulpaep, M., Kuemmerer, N., Lopez de la Paz, M., Martins, I.C., Reumers, J., Morris, K.L., Copland, A., Serpell, L., Serrano, L. *et al.* (2010) Exploring the sequence determinants of amyloid structure using position-specific scoring matrices. *Nature methods*, **7**, 237-242.

35   Kosten, J., Binolfi, A., Stuiver, M., Verzini, S., Theillet, F.X., Bekei, B., van Rossum, M. and Selenko, P. (2014) Efficient modification of alpha-synuclein serine 129 by protein kinase CK1 requires phosphorylation of tyrosine 125 as a priming event. *ACS chemical neuroscience*, **5**, 1203-1208.

36   Mukherjee, S., Chiu, R., Leung, S.M. and Shields, D. (2007) Fragmentation of the Golgi apparatus: an early apoptotic event independent of the cytoskeleton. *Traffic*, **8**, 369-378.

37   Taschenberger, G., Toloe, J., Tereshchenko, J., Akerboom, J., Wales, P., Benz, R., Becker, S., Outeiro, T.F., Looger, L.L., Bahr, M. *et al.* (2013) beta-synuclein aggregates and induces neurodegeneration in dopaminergic neurons. *Annals of neurology*, **74**, 109-118.

38   Ishikawa, K., Ishii, H. and Saito, T. (2006) DNA damage-dependent cell cycle checkpoints and genomic stability. *DNA and cell biology*, **25**, 406-411.

39   Bonda, D.J., Bajic, V.P., Spremo-Potparevic, B., Casadesus, G., Zhu, X., Smith, M.A. and Lee, H.G. (2010) Review: cell cycle aberrations and neurodegeneration. *Neuropathology and applied neurobiology*, **36**, 157-163.

40   Husseman, J.W., Nochlin, D. and Vincent, I. (2000) Mitotic activation: a convergent mechanism for a cohort of neurodegenerative diseases. *Neurobiology of aging*, **21**, 815-828.

41   Vivacqua, G., Casini, A., Vaccaro, R., Fornai, F., Yu, S. and D'Este, L. (2011) Different sub-cellular localization of alpha-synuclein in the C57BL\6J mouse's central nervous system by two novel monoclonal antibodies. *Journal of chemical neuroanatomy*, **41**, 97-110.

42   Yoshida, M. (2007) Multiple system atrophy: alpha-synuclein and neuronal degeneration. *Neuropathology : official journal of the Japanese Society of Neuropathology*, **27**, 484-493.

43   Kim, T., Mehta, S.L., Kaimal, B., Lyons, K., Dempsey, R.J. and Vemuganti, R. (2016) Poststroke Induction of alpha-Synuclein Mediates Ischemic Brain Damage. *J. Neurosci.*, **36**, 7055-7065.

44   Zhou, M., Xu, S., Mi, J., Ueda, K. and Chan, P. (2013) Nuclear translocation of alpha-synuclein increases susceptibility of MES23.5 cells to oxidative stress. *Brain Res*, **1500**, 19-27.

45   Galvin, J.E., Schuck, T.M., Lee, V.M. and Trojanowski, J.Q. (2001) Differential expression and distribution of alpha-, beta-, and gamma-synuclein in the developing human substantia nigra. *Experimental neurology*, **168**, 347-355.

46   Desplats, P., Spencer, B., Crews, L., Pathel, P., Morvinski-Friedmann, D., Kosberg, K., Roberts, S., Patrick, C., Winner, B., Winkler, J. *et al.* (2012) alpha-Synuclein induces alterations in adult neurogenesis in Parkinson disease models via p53-mediated repression of Notch1. *J. Biol. Chem.*, **287**, 31691-31702.

47   Vasudevaraju, P., Guerrero, E., Hegde, M.L., Collen, T.B., Britton, G.B. and Rao, K.S. (2012) New evidence on alpha-synuclein and Tau binding to conformation and sequence specific GC* rich DNA: Relevance to neurological disorders. *Journal of pharmacy & bioallied sciences*, **4**, 112-117.

48   Scheffold, A., Holtman, I.R., Dieni, S., Brouwer, N., Katz, S.F., Jebaraj, B.M., Kahle, P.J., Hengerer, B., Lechel, A., Stilgenbauer, S. *et al.* (2016) Telomere shortening leads to an acceleration of synucleinopathy and impaired microglia response in a genetic mouse model. *Acta neuropathologica communications*, **4**, 87.

49   Bukar Maina, M., Al-Hilaly, Y.K. and Serpell, L.C. (2016) Nuclear Tau and Its Potential Role in Alzheimer's Disease. *Biomolecules*, **6**, 9.

50   Saudou, F., Finkbeiner, S., Devys, D. and Greenberg, M.E. (1998) Huntingtin acts in the nucleus to induce apoptosis but death does not correlate with the formation of intranuclear inclusions. *Cell*, **95**, 55-66.

51   Kleinknecht, A., Popova, B., Lazaro, D.F., Pinho, R., Valerius, O., Outeiro, T.F. and Braus, G.H. (2016) C-Terminal Tyrosine Residue Modifications Modulate the Protective Phosphorylation of Serine 129 of alpha-Synuclein in a Yeast Model of Parkinson's Disease. *PLoS genetics*, **12**, e1006098.

52   Nicklas, S., Okawa, S., Hillje, A.L., Gonzalez-Cano, L., Del Sol, A. and Schwamborn, J.C. (2015) The RNA helicase DDX6 regulates cell-fate specification in neural stem cells via miRNAs. *Nucleic acids research*, **43**, 2638-2654.

53   Kugler, S., Meyn, L., Holzmuller, H., Gerhardt, E., Isenmann, S., Schulz, J.B. and Bahr, M. (2001) Neuron-specific expression of therapeutic proteins: evaluation of different cellular promoters in recombinant adenoviral vectors. *Molecular and cellular neurosciences*, **17**, 78-96.

54   Lopes da Fonseca, T., Pinho, R. and Outeiro, T.F. (2016) A familial ATP13A2 mutation enhances alpha-synuclein aggregation and promotes cell death. *Hum. Mol. Genet.*, **25**, 2959-2971.

55   Maddalena, A., Tereshchenko, J., Bahr, M. and Kugler, S. (2013) Adeno-associated Virus-mediated, Mifepristone-regulated Transgene Expression in the Brain. *Molecular therapy. Nucleic acids*, **2**, e106.

56   McKeith, I.G., Dickson, D.W., Lowe, J., Emre, M., O'Brien, J.T., Feldman, H., Cummings, J., Duda, J.E., Lippa, C., Perry, E.K. *et al.* (2005) Diagnosis and management of dementia with Lewy bodies: third report of the DLB Consortium. *Neurology*, **65**, 1863-1872.

57   Rockenstein, E., Mallory, M., Hashimoto, M., Song, D., Shults, C.W., Lang, I. and Masliah, E. (2002) Differential neuropathological alterations in transgenic mice expressing alpha-synuclein from the platelet-derived growth factor and Thy-1 promoters. *Journal of neuroscience research*, **68**, 568-578.

58   Fonseca-Ornelas, L., Eisbach, S.E., Paulat, M., Giller, K., Fernandez, C.O., Outeiro, T.F., Becker, S. and Zweckstetter, M. (2014) Small molecule-mediated stabilization of vesicle-associated helical alpha-synuclein inhibits pathogenic misfolding and aggregation. *Nature communications*, **5**, 5857.

59   Vranken, W.F., Boucher, W., Stevens, T.J., Fogh, R.H., Pajon, A., Llinas, M., Ulrich, E.L., Markley, J.L., Ionides, J. and Laue, E.D. (2005) The CCPN data model for NMR spectroscopy: development of a software pipeline. *Proteins*, **59**, 687-696.

60   Ross-Innes, C.S., Stark, R., Teschendorff, A.E., Holmes, K.A., Ali, H.R., Dunning, M.J., Brown, G.D., Gojis, O., Ellis, I.O., Green, A.R. *et al.* (2012) Differential oestrogen receptor binding is associated with clinical outcome in breast cancer. *Nature*, **481**, 389-393.

61   Love, M.I., Huber, W. and Anders, S. (2014) Moderated estimation of fold change and dispersion for RNA-seq data with DESeq2. *Genome biology*, **15**, 550.

62   Feng, J., Liu, T. and Zhang, Y. (2011) Using MACS to identify peaks from ChIP-Seq data. *Current protocols in bioinformatics*, **Chapter 2**, Unit 2 14.

63   Livak, K.J. and Schmittgen, T.D. (2001) Analysis of relative gene expression data using real-time quantitative PCR and the 2(-Delta Delta C(T)) Method. *Methods*, **25**, 402-408.

Legends to Figures

Fig 1. Expression of WT aSyn in cells promotes downregulation of genes associated with cell cycle. (A) Schematic representation of the generation of control and WT aSyn LUHMES cells. **(B)** Differentiated LUHMES cells showing highly homogeneous GFP-positive populations that exhibit extensive, TH-positive neuritic networks. Scale bar 100 μm. **(C)** Representative images of human H4 cells transfected with WT aSyn demonstrate that aSyn is distributed throughout the cell. Scale bar 50 μm. **(D)** Venn diagram displaying the number of cell cycle related genes found significantly deregulated in LUHMES and H4 cells upon expressing WT aSyn. **(E)** STRING protein network analysis showing the intricate interaction between cell cycle genes commonly deregulated in LUHMES and H4 cells. Genes coloured in red were selected for qPCR validation in H4 cells. **(F)** qPCR analysis confirmed a significant downregulation of *CCNB1*, *E2F8* and *MKI67* in H4 cells expressing WT aSyn, compared to control H4 cells. Data is expressed as mean ± SD; N=5. Unpaired t-test, two-tailed, p<0.05.

Figure 1

48
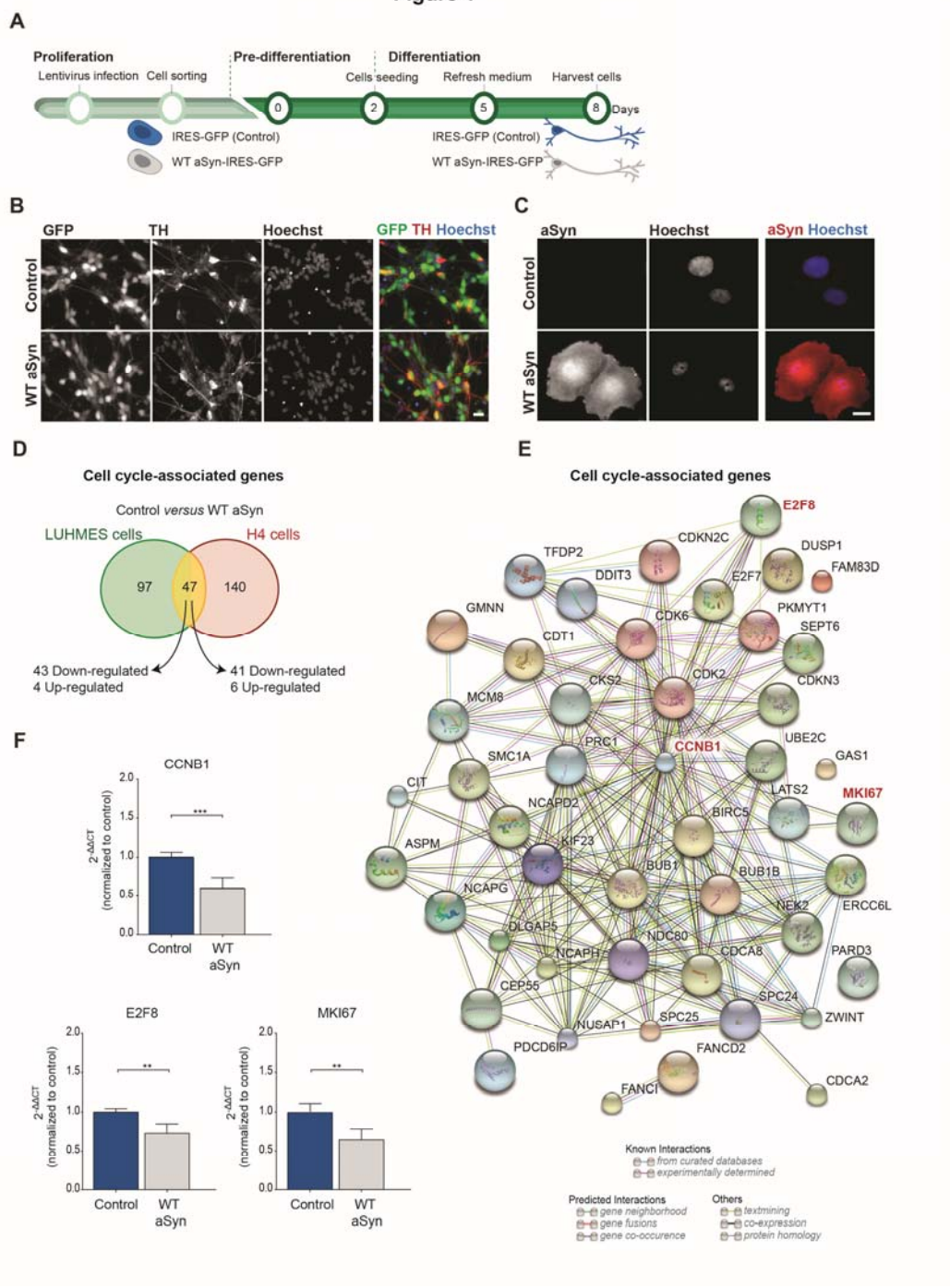
Fig 2. aSyn is present in the nucleus of cells from human and mouse samples. (A) Photomicrographs illustrating nuclear localization of aSyn (NCL-L), aSyn oligomers (5G4) and pS129 in the temporal lobe of a DLB patient. Scale bar = 180 μm **(B)** Representative images are provided for immunostainings of WT mNSC under maintenance conditions, or after 5 days of differentiation. mNSCs kept under maintenance conditions are positive for Nestin and express aSyn throughout the whole cell. In differentiated mNSC expressing Tuj1, aSyn signal was mostly localized in the nucleus. Scale bars = 20 μm. **(C)** Content of aSyn in cytoplasmic and nuclear fractions prepared from embryonic mice (E14), showing that 40% of aSyn is expressed in the nuclear fraction. **(D)** Analysis of aSyn content in cytoplasmic and nuclear extracts of 2 month old mice midbrain revealed that ~18% of aSyn is localized to the nucleus of young adult, WT mice while significantly higher levels are detected in age-matched transgenic mice overexpressing WT aSyn. **(E)** Similarly, aSyn levels in the nucleus of LUHMES cells were significantly higher in WT aSyn expressing cells, compared to control cells. **(F)** In transfected H4 cells, ~10% of total aSyn is localized in the nucleus. Data is expressed as mean ± SD; N=3. Unpaired t-test, two-tailed, p<0.05.

Figure 2

50
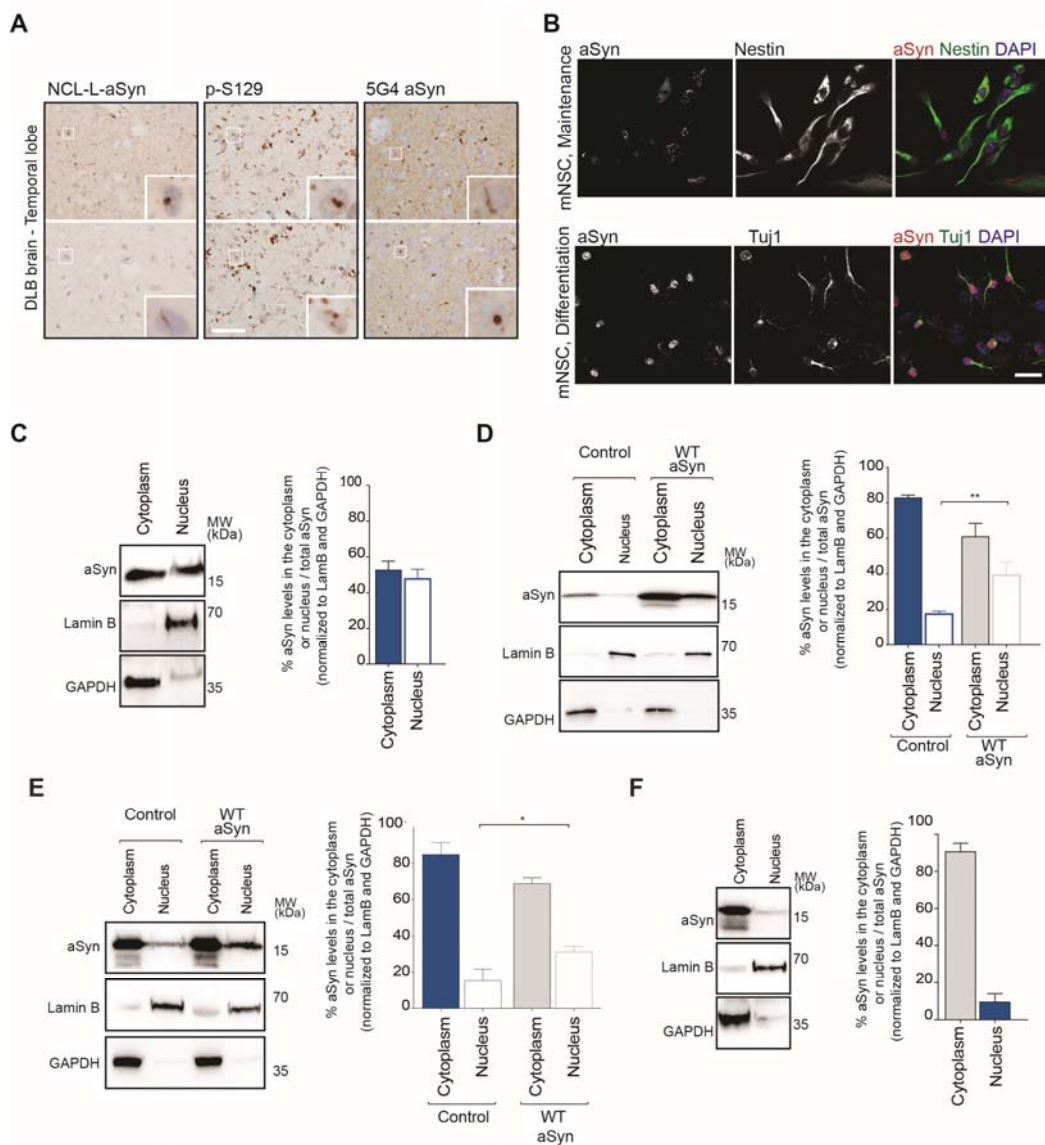
Fig 3. aSyn binds DNA *in vitro* and *in vivo* models of PD. (A) Changes in the position of NMR resonances in ^{15}N-labelled aSyn in the absence (grey) or presence (black) of annealed complementary primers (upper panel). Chemical shift changes in the bottom panel showing that, in the presence of a small DNA sequence, the NMR signal position changes for residues at the positively charged N-terminus, as well as for the amino acids at the negatively charged C-terminus. **(B)** ^{15}N-^{1}H HSQC spectra of aSyn were analysed in the absence (gray) and presence (black) of nucleosomes. Analysis of NMR chemical shift perturbations showed that residues at the N-terminus of aSyn interact with nucleosomes. **(C)** Volcano plot was obtained using genomic regions differentially bind by aSyn in control and WT aSyn LUHMES cells, in ChIP-seq. Red dots represent $p < 0.05$. Data showed that, in the control group, aSyn binds significantly more to DNA. **(D)** Volcano plot depicting differential binding of aSyn to genomic regions in transgenic WT aSyn mice and control mice. Grey dots represent $p < 0.05$. These analyses showed that aSyn significantly binds more DNA regions in the control group.

Figure 3

52
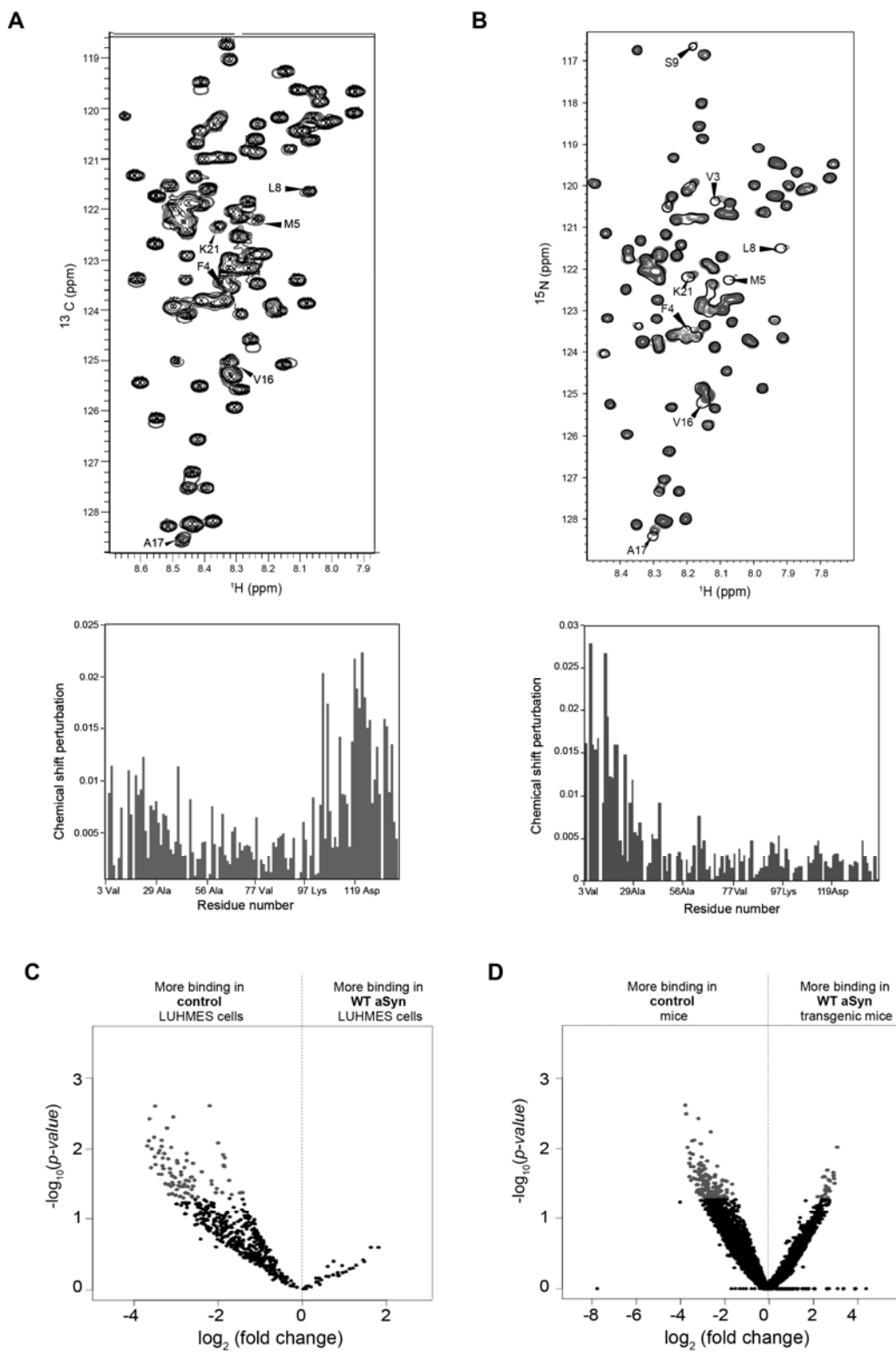
Fig 4. Nuclear aSyn is phosphorylated in S129. (A) Schematic representation of WT aSyn constructs used to express the protein in the cytoplasm or in the nucleus. **(B)** Levels of aSyn overexpression were confirmed using immunoblot analysis of total cell lysates. **(C)** Representative images of H4 cells transfected with each WT aSyn construct. WT aSyn is distributed in the whole cell, while cells expressing WT aSyn-NES lack aSyn immunoreactivity within the nucleus and display an accumulation of aSyn in the perinuclear areas (orange arrows heads). Cells expressing WT aSyn-NLS showed abundant aSyn signal in the nucleus and the presence of nuclear accumulations or inclusions (green arrows heads). Scale bar 50 μm. **(D)** Immunostaining showed a high abundance of aSyn-phosphorylated form in cells expressing WT aSyn-NLS. pS129 signals were mostly visualized within the nucleus. Scale bar 50 μm. **(E)** High magnification images demonstrating that WT aSyn nuclear inclusions, observed in cells expressing WT aSyn-NLS, stain positive for pS129 and are located in Hoechst-negative regions (green arrows heads). WT aSyn was also present and highly phosphorylated in mitotic spindles (asterisk). **(F)** Western blot analysis of pS129 aSyn levels, confirmed a significant increase of pS129 levels in WT aSyn-NLS cells. **(G)** The same set of samples were ran in SDS-PAGE, together with a positive control for pY125, and probed for pY125 showed no immunosignal. Data is expressed as mean ± SD; N=4. One-way ANOVA, with Bonferroni correction, $p < 0.05$.

Figure 4

54
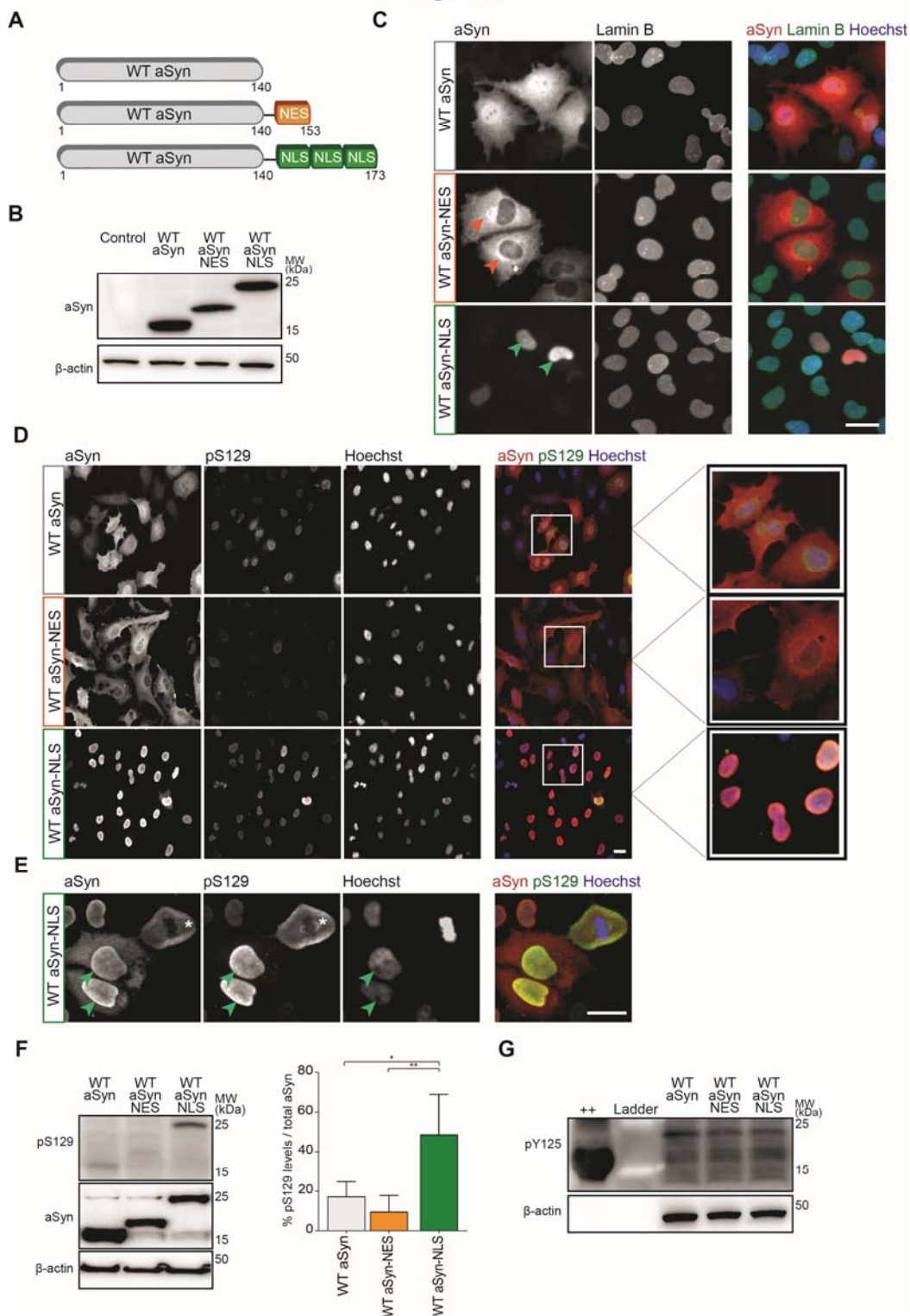
Fig 5. Nuclear localization of aSyn is dependent on phosphorylation in S129. (A) Plasmids encoding for WT aSyn, WT aSyn-NES and WT aSyn-NLS were used as template to generate identical constructs containing an alanine (A) substitution instead of serine (S) 129. **(B)** Immunoblot probed for pS129 aSyn showed a lack of signal in H4 cells expressing the S129A constructs. **(C)** Representative images of H4 cells transfected with each WT aSyn variant. S129A aSyn was either distributed throughout cell or solely in the cytoplasm, whereas the WT aSyn showed a more homogeneous distribution. Similarly, S129A aSyn-NLS showed an increase of aSyn signal in the cytoplasm, compared to its WT form. Both WT aSyn-NES and S129A aSyn-NES were localized in the cytoplasm, with preferential accumulation in perinuclear regions. Scale bar 50 μm. **(D)** Immunoblot quantification of cytoplasmic and nuclear fractions from H4 cells expressing each aSyn form confirmed that the levels of aSyn in the nucleus of cells expressing S129 aSyn and S129A aSyn-NLS was significantly lower when compared to the WT form. **(E)** On native gels analysis, three distinct bands were detected for WT aSyn, S129A aSyn, WT aSyn-NES and S129A aSyn-NES (~20 kDa, 45 kDa and ~145 kDa). aSyn with high molecular weight was observed in samples from cells expressing WT aSyn-NLS. S129A aSyn-NLS expressing cells showed a similar pattern and the presence of a smear at ~50kDa. Each immunoblot provided is representative of N=3, except data on native gel which corresponds to an N=2. Unpaired t-test, two-tailed, $p < 0.05$.

Figure 5
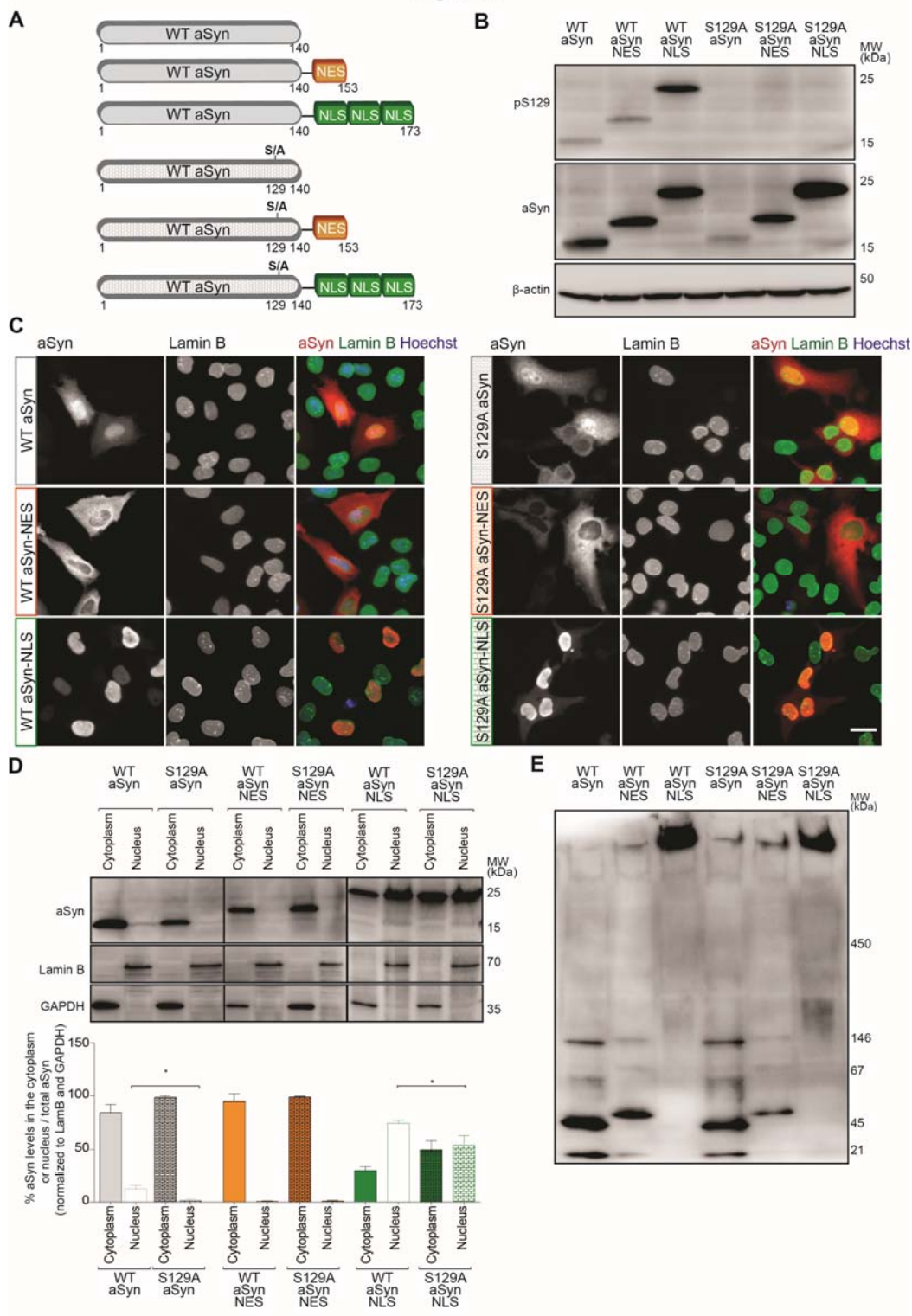
Fig 6. aSyn subcellular localization and pS129 phosphorylation alter its half-life, sensitivity to PK and effect on transcription. (A) Lysates from H4 cells expressing WT aSyn, WT aSyn-NES or WT aSyn-NLS were digested with PK for 0, 5 or 10 minutes. Analysis showed significant lower resistance of WT aSyn-NES to PK treatment. **(B)** Blocking aSyn and aSyn-NES S129 phosphorylation led to a significantly faster PK digestion. The reverse effect was detected for aSyn-NLS. **(C)** H4 cells expressing WT aSyn constructs were treated with CHX for 12 or 24h. At 12h of CHX treatment WT aSyn-NLS cells expressed significantly higher amounts of aSyn compared to WT-NES and, 12h later, to WT aSyn and WT aSyn-NES. **(D)** Blocking phosphorylation did not produce significant differences in the expression levels of WT aSyn and WT aSyn-NLS along CHX treatment, while S129A aSyn-NES showed shorter half-life at 12h of CHX treatment, compared to the WT form. Data is expressed as mean ± SD; N=3. Two-way ANOVA, with Bonferroni correction, $p < 0.05$. **(E)** qPCR analysis show that expression of WT aSyn-NLS promoted a significant up-regulation of *CCNB1*, compared to both WT aSyn and WT aSyn-NES, and a significant up-regulation of *E2F8* and *MKI67* compared to WT aSyn-NES. **(F)** Gene expression levels were compared between each WT and its S129A construct. Increases in fold-change for *CCNB1* and *E2F8* were detected when expressing S129A aSyn, compared to the WT aSyn. An identical effect was observed when comparing S129A aSyn-NES and WT aSyn-NES, while the reverse was observed when expressing S129A aSyn-NLS. Data is expressed as mean ± SD; N=5. One-way ANOVA, with Bonferroni correction, was used for statistical analysis between WT aSyn constructs, $p < 0.05$. Statistical analyses between WT and S129A aSyn forms was performed using Unpaired t-test, two-tailed, $p < 0.05$.

Figure 6

58
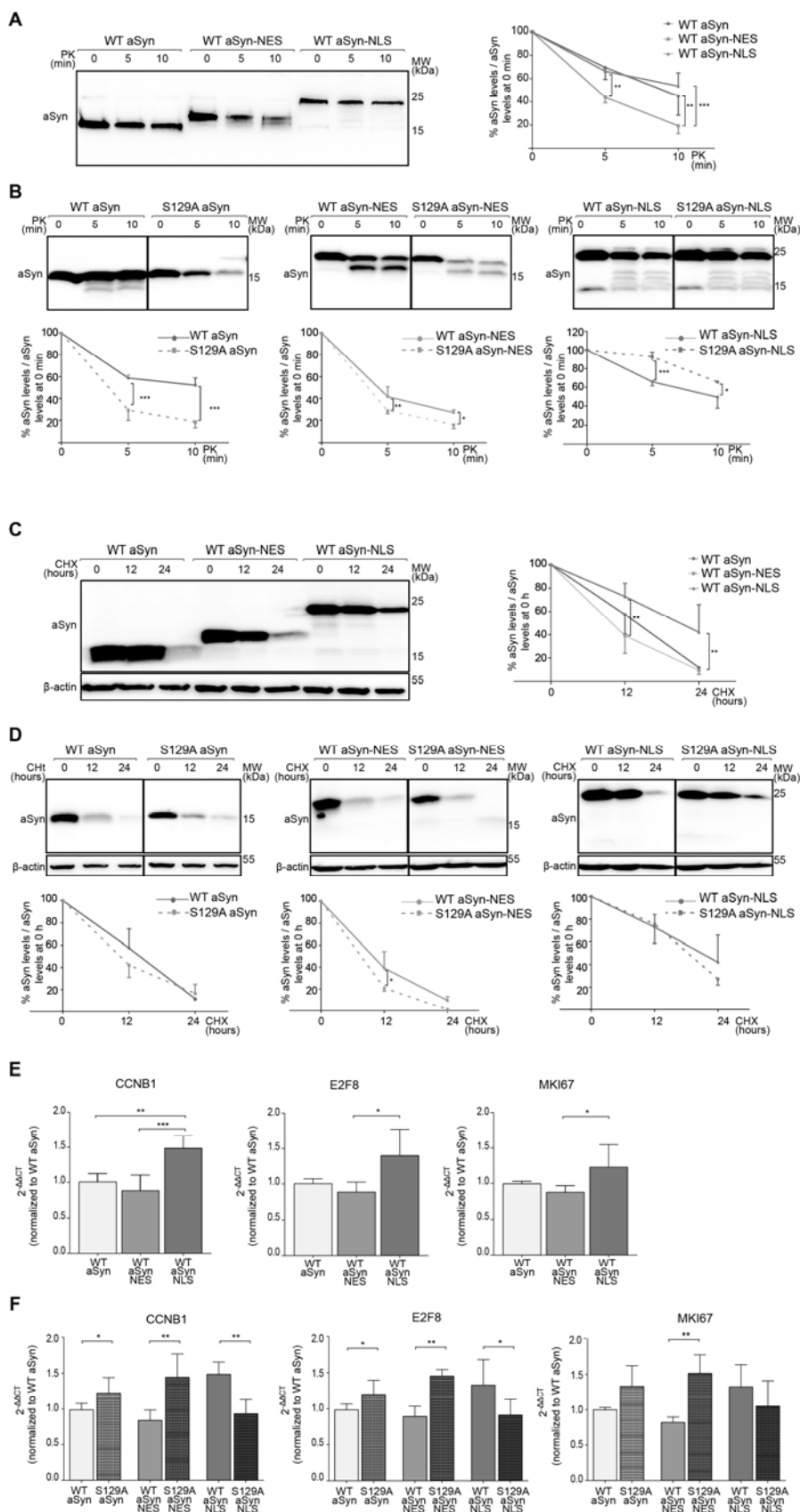
Fig 7. Nuclear localization of WT aSyn reduces cell damage. **(A)** Representative images are provided showing aSyn and Giantin expression in H4 cells transfected with each WT construct. **(B)** Golgi morphology was classified as fragmented or non-fragmented. Statistical analyses showed that when aSyn was expressed in the nucleus (WT aSyn-NLS) less cells presented fragmented Golgi, compared to cells expressing WT aSyn or WT aSyn-NES. When expressing WT aSyn-NES, the number of cells with fragmented Golgi was significantly higher than the number of cells with normal Golgi morphology. **(C)** S129A WT aSyn-NLS displayed increased number of cells with fragmented Golgi, compared to cells expressing the WT form. The reverse effect was observed when blocking S129 phosphorylation of WT aSyn and WT aSyn-NES (N=3). **(D)** Expressing WT aSyn in the cytoplasm (WT aSyn-NES) also led to a significantly higher percentage of cells positive for c-casp3, compared to cells expressing WT aSyn or WT aSyn-NLS. **(E)** Statistical analyses between WT and S129 forms showed that blocking WT aSyn and WT aSyn-NES S129 phosphorylation reduced the percentage of apoptotic cells. In contrast, expressing S129A aSyn-NLS promoted casp3 cleavage in a higher percentage of cells, compared to its WT form (N=5). **(F)** WT aSyn-NLS promoted a reduction in the number of TUNEL positive cells compared to WT aSyn and WT aSyn-NES. DNA fragmentation was also significantly higher in WT aSyn-NES cells compared to WT aSyn cells. **(G)** Similar experiments comparing WT and S129A aSyn forms showed that S129A aSyn and S129A aSyn-NES promoted a lower percentage of aSyn expressing cells with fragmented DNA. The reverse effect was observed when WT aSyn-NLS S129 phosphorylation was blocked (N=4). **(H)** DNA fragmentation was further investigated using the comet assay alkali method. Representative images of PI-stained comets are provided for each condition. **(I)** Tail moments from H4 cells expressing WT aSyn-

NES were significantly higher than those from cells expressing WT aSyn or WT aSyn-NLS. **(J)** WT aSyn and WT aSyn-NES expressing cells displayed larger tail moments when compared to cells expressing its S129A forms. The reverse was observed when expressing S129A aSyn-NLS (N=4). **(K)** Bioluminescence measurements of AK performed with Toxilight assay showed a significant increase of cellular toxicity when expressing WT aSyn-NES. **(L)** Furthermore, expression of S129A aSyn and S129A aSyn-NES produced less toxicity compared to its WT form (N=5). Data is expressed as mean ± SD of, at least, N=3. One-way ANOVA, with Bonferroni correction, was used for statistical analysis between WT aSyn constructs, $p < 0.05$. Statistical analyses between WT and S129A aSyn forms was performed using Unpaired t-test, two-tailed, $p < 0.05$.

Figure 7
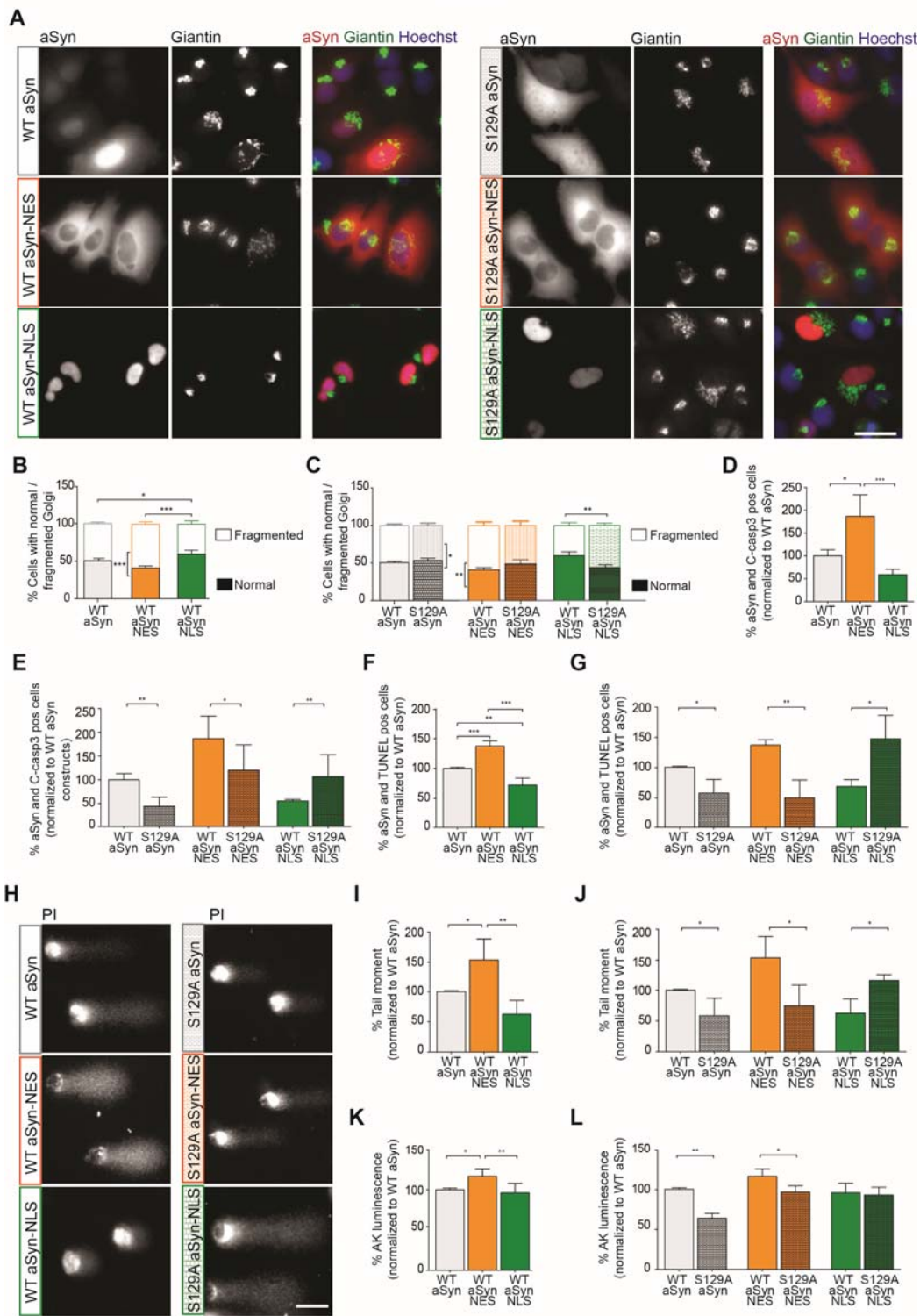
Abbreviations

AAV - Adeno-associated virus

AD - Alzheimer's disease

aSyn – Alpha-synuclein

aSyn-NES - aSyn linked to a nuclear export signal

aSyn-NLS - aSyn linked to a nuclear localization sequence

BiFC - Bimolecular fluorescence complementary

c-casp3 - Cleaved of caspase 3

CCNB1 - Cyclin B1

ChIP-seq - Chromatin immunoprecipitation followed by next-generation sequencing

CHX - Cycloheximide

DLB – Dementia with Lewy bodies

E14 - Day 14 of embryonic stage

E2F8 - E2F Transcription Factor 8

LUHMES - Lund human mesencephalic

MKI67 - Proliferation Marker Protein Ki-67

mNSC - Mouse neuronal stem cells

NMR - Nuclear magnetic resonance

PD - Parkinson's disease

PGC1-alpha - Peroxisome proliferator-activated receptor gamma coactivator 1-alpha

PK - Proteinase K

pS129 - Phosphorylation of aSyn at serine S129

PTMs - Posttranslational modifications

qPCR – Real-time PCR

S129A –Substitution of serine at position 129 by an alanine

SD – Standard deviation

TH - Tyrosine hydroxylase

Tuj1 - β-tubulin III

WT - Wild-type